Journal of Medicinal Chemistry

Article

Novel Mechanism of Cytotoxicity for the Selective Selenosemicarbazone, 2-Acetylpyridine 4,4-Dimethyl-3-Selenosemicarbazone (Ap44mSe): Lysosomal Membrane Permeabilization

Zaynab Al-Eisawi, Christian Stefani, Patric Jansson, Akanksha Arvind, Philip C Sharpe, Maram Basha, George M Iskander, Naresh Kumar, Zaklina Kovacevic, Darius J.R. Lane, Sumit Sahni, Paul Vincent Bernhardt, Des R Richardson, and Danuta Sandra Kalinowski

J. Med. Chem., **Just Accepted Manuscript** • DOI: 10.1021/acs.jmedchem.5b01399 • Publication Date (Web): 08 Dec 2015

Novel Mechanism of Cytotoxicity for the Selective Selenosemicarbazone, 2-Acetylpyridine 4,4-Dimethyl-3-Selenosemicarbazone (Ap44mSe): Lysosomal Membrane Permeabilization

Zaynab Al-Eisawi[†], Christian Stefani[†], Patric J. Jansson[†], Akanksha Arvind[†], Philip C. Sharpe[‡], Maram T. Basha[‡], George M. Iskander[^], Naresh Kumar[^], Zaklina Kovacevic[†], Darius J.R. Lane[†], Sumit Sahni[†], Paul V. Bernhardt[‡*], Des R. Richardson[†*] and Danuta S. Kalinowski[†*]

[†]*Molecular Pharmacology and Pathology Program, Department of Pathology, The University of Sydney, Sydney, NSW, 2006, Australia*

[‡]*School of Chemistry and Molecular Biosciences, University of Queensland, Brisbane, QLD, 4072, Australia*

[^]*School of Chemistry, University of New South Wales, Sydney, NSW, 2052, Australia*

Abstract

Selenosemicarbazones show marked anti-tumor activity. However, their mechanism of action remains unknown. We examined the medicinal chemistry of the selenosemicarbazone, 2-acetylpyridine 4,4-dimethyl-3-selenosemicarbazone (Ap44mSe), and its iron and copper complexes to elucidate its mechanisms of action. Ap44mSe demonstrated a pronounced improvement in selectivity towards neoplastic relative to normal cells compared to its parent thiosemicarbazone. It also effectively depleted cellular Fe, resulting in transferrin receptor-1 up-regulation, ferritin down-regulation and increased expression of the potent metastasis suppressor, N-myc downstream regulated gene-1. Significantly, Ap44mSe limited deleterious methemoglobin formation, highlighting its usefulness in overcoming toxicities of clinically-relevant thiosemicarbazones. Furthermore, Cu-Ap44mSe mediated intracellular reactive oxygen species generation, which was attenuated by the anti-oxidant, *N*-acetyl-L-cysteine, or Cu sequestration. Notably, Ap44mSe forms redox active Cu complexes that target the lysosome to induce lysosomal membrane permeabilization. This investigation highlights novel structure-activity relationships for future chemotherapeutic design, and underlines the potential of Ap44mSe as a selective anti-cancer/anti-metastatic agent.

Introduction

Trace metals, including iron (Fe) and copper (Cu), are elements that are vital for normal cellular function.[1-3] The participation of Fe and Cu in a wide range of cellular processes is due to their innate ability to redox cycle and act as both electron donors and acceptors.[2] For example, Fe has crucial roles in oxygen transport, electron transfer, energy metabolism, DNA synthesis and cell cycle progression.[2,3] Moreover, Fe acts as a cofactor for the key enzyme, ribonucleotide reductase (RR), that catalyzes the reduction of ribonucleotides to deoxyribonucleotides and is the rate-limiting step in DNA synthesis.[1] Due to their rapid cell growth and proliferation, it is not entirely surprising that Fe is crucial for the proliferation of cancer cells.[4]

It is also well recognized that Cu is vital for the activity of many enzymes essential for cellular respiration, defense against reactive oxygen species (ROS), melanin synthesis, formation of connective tissue and Fe metabolism.[5] It is also an essential co-factor for tumor angiogenesis[6,7] and metastasis.[8] In fact, Fe and Cu metabolism is profoundly altered in many human cancers.[5,9] Considering the crucial roles of these metals, the development of novel agents that target Fe and Cu have become a promising anti-cancer strategy.

Chelators, such as desferrioxamine (DFO, Fig. 1A), have been traditionally used for the treatment of Fe overload disease. Early studies investigating the anti-tumor efficacy of DFO demonstrated only modest efficacy *in vitro* and *in vivo*.[2,10] The limited membrane permeability of DFO resulted in poor anti-cancer activity and prevented its application in cancer therapy.[11,12] Recently, a number of studies have demonstrated that thiosemicarbazone chelators are an evolving class of agents, with di-2-pyridylketone 4,4-dimethyl-3-thiosemicarbazone (Dp44mT; Fig. 1B) showing effective and selective anti-tumor activity *in vitro* and *in vivo* that can overcome resistance to conventional chemotherapy.[13,14]

The anti-proliferative activity of more potent chelators, such as Dp44mT and those of the 2-acetylpyridine thiosemicarbazone series, such as 2-acetylpyridine 4,4-dimethyl-3-thiosemicarbazone (Ap44mT; Fig. 1C),[15] is likely mediated by their effects on multiple molecular targets.[16] In addition to binding to Fe, thiosemicarbazones possess the ability to bind Cu.[17-19] The resultant Fe and Cu complexes are capable of engaging in redox cycling to generate ROS, such as hydroxyl radicals, *via* the Fenton reaction.[18-20] These ROS mediate cellular injury to induce apoptosis.[2,18,19]

Other modes of anti-cancer activity mediated by thiosemicarbazones include the up-regulation of the metastasis suppressor protein, N-myc downstream regulated gene-1 (NDRG1)[21-23] and the inhibition of cell cycle progression (G_1/S phase) through the modulation of the expression of the cyclin family of proteins (*e.g.*, cyclin D1),[24] GADD family of proteins (*e.g.*, GADD45),[25] and cyclin-dependent kinase 2.[26] Furthermore, the accumulation of Cu thiosemicarbazone complexes in the lysosome activates the lysosomal apoptotic pathway through lysosomal membrane permeabilization (LMP).[19] The induction of LMP causes the proteolytic activation of Bid, which is cleaved by the lysosomal cathepsins, B and D, to subsequently induce mitochondrial outer membrane permeabilization, resulting in cytochrome *c* release and apoptosome-dependent caspase activation, and ultimately, apoptosis.[27-29]

Studies have highlighted the potential of chalcogensemicarbazones, such as selenosemicarbazones as anti-cancer agents.[30-34] The substitution of chalcogen atoms with selenium in chalcogensemicarbazones resulted in increased activity as anti-bacterial, anti-parasitic and anti-viral agents.[35-37] Selenosemicarbazones and their Pt(II) and Pd(II) complexes were also found to demonstrate marked anti-tumor activity *in vitro*.[31,33,34] These results demonstrated the potential application of selenosemicarbazones as novel compounds in cancer therapy.

We investigated the impact of substituting the thiocarbonyl sulfur in Ap44mT (Fig. 1C) with selenium to generate, 2-acetylpyridine 4,4-dimethyl-3-selenosemicarbazone (Ap44mSe; Fig. 1D), in an effort to develop highly potent, yet well tolerated, anti-cancer agents and gain further insight into the structure-activity relationships of selenosemicarbazones. In this study, we examined the electrochemical and intracellular behavior of Ap44mSe (Fig. 1D) and its Fe and Cu complexes in SK-N-MC neuroepithelioma cells. Herein, it is demonstrated that the anti-proliferative activity of Ap44mSe is linked with the ability of its resultant Cu complex to redox cycle, leading to intracellular ROS generation and LMP. Our findings underline for the first time the importance of ROS generation and LMP in the anti-cancer activity of Ap44mSe and demonstrate lysosomal targeting as a novel mechanism of selenosemicarbazone anti-proliferative activity. Moreover, substitution of thiocarbonyl S for Se in Ap44mSe, resulted in markedly higher anti-tumor selectivity and lower metHb generation relative to its parent thiosemicarbazone and a lead di-2-pyridylketone thiosemicarbazone, Dp44mT. The novel structure-activity relationships highlighted herein are important for future chemotherapeutic design.

Results and Discussion

Synthesis and Structural Characterization

2-Acetylpyridine 4,4-dimethyl-3-selenosemicarbazone (Ap44mSe) was prepared by *S*-methylation of Ap44mT with methyl iodide in the presence of a base.[38] This was followed by substitution of the *S*-methyl group by selenium using sodium hydrogen selenide under argon.[38] The Cu^{II} complexes were prepared following methods employed previously for Ap44mT and its complexes.[18] Using cupric acetate provides both a coordinating co-ligand and a base to deprotonate the NH group of the selenosemicarbazone, which coordinates in its imino-selenolate anionic form. The IR spectrum of this complex reveals the presence of coordinated acetate (1607 cm^{-1}) in addition to several other strong IR bands from the coordinated ligand. The ligand and Cu^{II} complexes exhibit good solubility in MeCN and DMF. Further development of the hydrochloride salt of Ap44mSe would enhance aqueous solubility for future assessment in preclinical studies.

As an appropriate example, the crystal structure of [Cu(Ap44mSe)(OAc)] was determined. A view of the molecule is shown in Fig. 2A and selected bond lengths are in Table 1. The Cu atom is in a distorted square planar coordination geometry comprising the coordinated *N, N, Se*- donor set of the deprotonated selenosemicarbazone and a monodentate coordinated acetato ligand. The second acetate O-atom (O2) is more than 2.8 Å from the Cu ion and there are no other closer contacts with the metal (Fig. 2A).

There are some interesting parallels with the structure of the homologous thiosemicarbazone Cu complex of Ap44mT, namely [Cu(Ap44mT)(OAc)].[18] The larger covalent radius of Se compared to S lengthens both the Cu-X (X= Se, S) and C8-X bond lengths by around 0.13 Å. This has an influence on the coordinate angles as well. The *trans* coordinate angle N1-Cu-X1 is effectively set by the rigid ligand and decreases further away from linearity in [Cu(Ap44mSe)(OAc)] due to the

longer Cu-Se and C8-Se bonds. The C8-Se-Cu bond is close to 90° (*ca.* 3° smaller than the S-donor in its analogous thiosemicarbazone), which is expected for the heavier chalcogen donor atom.

When cupric perchlorate was used as a precursor in the presence of a 1:2 Cu:ligand ratio, the expected bis-selenosemicarbazone complex was not obtained, but instead an unusual dinuclear Se-bridged complex was isolated. Its crystal structure was determined and a view of the complex cation appears in Fig. 2B. The structure comprises two Cu ions and three selenosemicarbazone ligands; two of them connecting the Cu ions *via* Cu-Se-Cu bridges. The environment of Cu1 resembles bis-thiosemicarbazone complexes such as [Cu(Ap44mT)$_2$], where a tetragonally elongated (Jahn-Teller distorted) 6-coordinate geometry is present.[18] The elongated axis is defined by the *trans* donor atoms, N1B and Se1B, from ligand 'B', whose bonds to Cu1 are elongated by more than 0.2 Å compared to the corresponding N1A and Se1A donor atoms of ligand 'A' (Table 2). The environment of Cu2 is different and the metal is in a pseudo-square planar environment, comprising an unusual N_2Se_2 donor set with an additional bridging Se atom (Se1A) at the apex. However, Se1A is approximately 0.5 Å further from the Cu than the equatorially coordinated Se donors (Se1B and Se1C) and formally within the coordination sphere (Fig. 2B). The environment of Cu2 resembles the geometry found in [Cu(Ap44mSe)(OAc)], where Se1B replaces the equatorial acetate.

Electrochemistry

The electrochemical properties of [Cu(Ap44mSe)(OAc)] and [Cu$_2$(Ap44mSe)$_3$](ClO$_4$) were investigated in MeCN:H$_2$O (70:30 v/v). These complexes exhibit good solubility in MeCN and DMF, but are not soluble in water alone at millimolar concentrations. The solvent mixture of MeCN:H$_2$O (70:30 v/v) provided a good compromise. Indeed, it enabled the electrochemical properties to be studied under conditions where a high concentration of water was present, and thus, these conditions are more biologically relevant than investigations in pure organic solvent.

Furthermore, this solvent combination has been utilized in our previous studies on other thiosemicarbazone systems[15,17,39,40] enabling a useful comparison.

The mononuclear complex [Cu(Ap44mSe)(OAc)] yielded a quasi-reversible $Cu^{II/I}$ redox couple at -220 mV *vs.* the NHE (Fig. 3A). This $Cu^{II/I}$ redox potential is similar to that found in the complex [Cu(Ap44mT)(OAc)] (-204 mV *vs.* the NHE).[18] On the initial sweep (data not shown), a higher potential pre-wave was seen which disappears on subsequent cycles. The data shown in Fig. 3A correspond to the second cycle. Under these conditions (30% water), hydrolysis of the acetate ligand most likely occurs.

The dinuclear complex $[Cu_2(Ap44mSe)_3](ClO_4)$ was also examined under the same conditions. The two Cu centers bear very different coordination environments (Fig. 2B). In the solid state, one Cu ion is chelated by two Ap44mSe ligands, while the other is only coordinated by one selenosemicarbazone and resembles [Cu(Ap44mSe)(OAc)]. The cyclic voltammetry of this dinuclear complex demonstrates two well-separated, quasi-reversible $Cu^{II/I}$ couples at -217 and -461 mV *vs.* the NHE (Fig. 3B). By analogy with the cyclic voltammetry of [Cu(Ap44mSe)(OAc)] (Fig. 3A), the higher potential couple is assigned to the 1:1 Cu:L component, while the lower potential couple is attributed to the CuL_2 moiety. Interestingly, there is no significant difference between the higher redox potential of $[Cu_2(Ap44mSe)_3](ClO_4)$ and that found for [Cu(Ap44mSe)(OAc)]. Normally, the proximity of another Cu ion bridged by two Se atoms would be expected to raise the $Cu^{II/I}$ redox potential, but it is unchanged. This suggests that the dinuclear complex dissociates in solution to generate $[Cu(Ap44mSe)_2]$ and $[Cu(Ap44mSe)(OH_2)]^+$ in the presence of water.

We have previously found that 1:2 Cu^{II}:thiosemicarbazone complexes from this family partially dissociate to give a mixture of 1:1 and 1:2 Cu:ligand complexes due to a Jahn-Teller distortion that weakens a pair of *trans* axial coordinate bonds in the 6-coordinate Cu^{II} state.[18] In the present case,

the initial cathodic sweep produced two $Cu^{II/I}$ peaks of equal magnitude (Fig. 3C), which illustrates that the putative separated $[Cu^{II}(Ap44mSe)(OH_2)]^+$ and $[Cu^{II}(Ap44mSe)_2]$ complexes are stable. In the second voltammetric cycle, the magnitude of the $[Cu(Ap44mSe)(OH_2)]^{+/0}$ couple increases relative to the lower potential $[Cu(Ap44mSe)_2]^{0/-}$ wave (Fig. 3C). This is indicative of partial dissociation of $[Cu^{I}(Ap44mSe)_2]^-$ to liberate free ligand and more $[Cu^{I}(Ap44mSe)(OH_2)]$ at the electrode surface; only reduction to Cu^I triggers partial ligand dissociation. This chemical reaction coupled to electron transfer proceeds relatively slowly and the rate of the reaction may be followed at different sweep rates (Fig. 3C). At rapid sweep rates (100 mV s^{-1} and above), the first and second cycles are not significantly different and no dissociation can occur on this timescale. However, at 25 and 50 mV s^{-1} the higher potential cathodic wave is significantly enhanced on the second cycle due to the ligand dissociation from Cu^I proceeding to a greater extent (Fig. 3C).

EPR Spectroscopy

Electron paramagnetic spectroscopy is a particularly useful technique for interrogating the coordination geometry of Cu^{II} complexes. The frozen (DMF) solution X-band EPR spectrum of [Cu(Ap44mSe)(OAc)] is shown in Figure 4. The spectrum is rich in fine structure. Hyperfine coupling between the single electron spin and both the Cu nucleus (I = 3/2) and the *cis* N-donors (I = 1) is apparent. The spin Hamiltonian parameters were obtained by spectral simulation (see Supporting Information Fig. S1). For comparison, the EPR spectrum of [Cu(Ap44mT)(OAc)] (published previously)[18] is shown and clearly the two spectra are quite similar. Both are characteristic of a mononuclear Cu^{II} complex in a pseudo-square planar $N_2OS(e)$ coordination environment. The similarity of the g values and hyperfine coupling constants indicates that substitution of Se for S has only a small effect on the EPR properties. Also, the only Se isotope with non-zero spin is ^{77}Se (I = ½), but it is only 7.6% abundant,[41] and thus, no additional hyperfine coupling was resolved.

Interestingly, the dinuclear complex $[Cu_2(Ap44mSe)_3](ClO_4)$ is EPR silent. It is important to note that EPR was carried out in DMF, so the dinuclear complex is evidently persistent in the absence of water, in contrast to the electrochemistry in mixed aqueous solvent. The fact that the two d^9 metal centers are bridged by the two Se-donors leads to strong anti-ferromagnetic coupling and no EPR spectrum.

Biological Studies

Ap44mSe Demonstrates Anti-Proliferative Activity Against Tumor Cells that is Much Greater than DFO, but Similar to Ap44mT and Dp44mT

The ability of the selenosemicarbazone, Ap44mSe, to inhibit cellular proliferation was assessed using SK-N-MC neuroepithelioma cells, as the effect of other chelators and thiosemicarbazones on its growth has been well characterized.[15,40,42] The activity of Ap44mSe was compared to the parent compound, Ap44mT,[15] and two positive control chelators (Table 2), which included: **(1)** DFO, that is used for Fe overload therapy;[2] and **(2)** Dp44mT, a thiosemicarbazone with marked anti-proliferative activity (Fig. 1).[13,40,43]

The selenosemicarbazone, Ap44mSe, showed potent anti-proliferative efficacy against SK-N-MC cells, with an IC_{50} value of 0.011 μM (Table 2). In comparison, the parent ligand, Ap44mT, also demonstrated marked anti-cancer activity (0.009 μM; Table 2). Dp44mT showed the greatest anti-proliferative efficacy of all the ligands examined, with an IC_{50} value of 0.007 μM that was significantly ($p < 0.001$) lower than that of DFO, and slightly less than that for Ap44mT and Ap44mSe (Table 2). The clinically used agent, DFO, demonstrated poor anti-proliferative effects, with an IC_{50} of 19.31 μM (Table 2), which was similar to previously observed results.[15,39] This study highlights the potent anti-proliferative activity of the selenosemicarbazone, Ap44mSe.

The Cu Complexes of Ap44mSe, But Not its Fe Complex, Demonstrate Similar Activity to the Ligand Alone

Previous studies have illustrated that complexation of chelators with metals can result in significant changes in their biological activity.[18,19,40] To determine the effect of complexation on the anti-proliferative behavior of Ap44mSe, the 1:2 Fe:ligand complex and the 1:1 and 1:2 Cu:ligand complexes were prepared and their anti-proliferative activity was examined using SK-N-MC neuroepithelioma cells relative to the Fe and Cu complexes of the ligands, DFO, Dp44mT and Ap44mT (Table 2).

In comparison with their free ligands, the Fe complexes of all the chelators demonstrated poor anti-proliferative activity and resulted in IC_{50} values of >25 μM for the 1:1 DFO-Fe complex and >0.8 μM for 2:1 ligand to Fe complexes of Dp44mT, Ap44mT and Ap44mSe (Table 2). The Cu complexes of DFO demonstrated IC_{50} values that were slightly, but significantly (p < 0.01-0.05) less than the ligand alone, namely 11.44-11.81 μM relative to 19.31 μM (Table 2). On the other hand, the anti-proliferative activity of the Cu complexes of Dp44mT, Ap44mT and Ap44mSe were either similar to (p > 0.05), or significantly (p < 0.001-0.01) less than, their respective ligands (Table 2). Notably, unlike the Fe complex, the Cu complexes of Ap44mSe (*i.e.*, 1:1 and 2:1 ligand:metal complex) retained similar (p > 0.05) anti-proliferative activity as the ligand (Table 2), suggesting Cu complexation may play a role in the anti-proliferative efficacy of Ap44mSe.

Ap44mSe Demonstrates Markedly Greater Selective Anti-Proliferative Activity (Therapeutic Index) Against Tumor Cells Versus Normal Mortal Cells Relative to Ap44mT or Dp44mT

The selective anti-proliferative efficacy of Ap44mSe relative to Dp44mT and Ap44mT towards neoplastic cells was assessed by comparing SK-N-MC neuroepithelioma cells to mortal MRC-5 fibroblasts (Table 3). Their selectivity was assessed by calculating an *in vitro* therapeutic index (Table 3). This parameter represents the ratio of the IC_{50} values of normal to neoplastic cells (*i.e.*,

IC_{50} (MRC-5)/IC_{50} (SK-N-MC); Table 3), with higher values representing greater selectivity towards cancer cells.

Neoplastic cells were found to be markedly and significantly ($p < 0.01$-0.05) more sensitive than normal MRC-5 cells to the anti-proliferative activity of Ap44mT, Dp44mT and Ap44mSe (Table 3). Of the ligands examined herein, Ap44mSe was found to be the most selective, based on an IC_{50} value of 2.10 μM against MRC-5 cells and 0.011 μM against SK-N-MC cells (Table 3). Both Dp44mT and Ap44mT demonstrated similar anti-proliferative activity towards MRC-5 cells, resulting in IC_{50} values of 0.54 and 0.45 μM, respectively, and therapeutic indices of 77 and 50, respectively (Table 3). Importantly, although Ap44mSe demonstrated slightly decreased anti-proliferative effects against SK-N-MC cells relative to Dp44mT and Ap44mT, it showed the greatest selectivity of all the ligands examined (Table 3), and this property highlights its potential as a selective anti-cancer agent.

Ap44mSe Demonstrates ^{59}Fe Mobilization Efficacy from Cells that is Markedly Greater than DFO and Similar to that of Ap44mT and Dp44mT

As the ability of chelators to bind Fe from critical cellular Fe pools plays a role in their anti-tumor activity,[42] the ability of Ap44mSe to mobilize intracellular ^{59}Fe from prelabeled SK-N-MC neuroepithelioma cells was examined (Fig. 5A). The efflux of cellular ^{59}Fe mediated by Ap44mSe was compared to that of DFO, Dp44mT and Ap44mT, which have been characterized in this cell-type[15,39,40] and did not induce apoptosis during the short incubation period utilized.

As shown previously,[15,40] control medium alone led to very little ^{59}Fe efflux from cells, namely 3.7% of intracellular ^{59}Fe (Fig. 5A). Similarly, DFO at 2.5 and 25 μM also demonstrated limited ability to mobilize ^{59}Fe, resulting in the release of 3.8% and 6.2% of cellular ^{59}Fe, respectively.[15,40] In contrast, incubation of SK-N-MC cells with either Dp44mT and Ap44mT at 2.5 or 25 μM led to

a significant ($p < 0.001$) increase in ^{59}Fe mobilization efficacy relative to the control, resulting in the efflux of 32-34% of cellular ^{59}Fe (Fig. 5A). Similarly, Ap44mSe also mediated significantly ($p < 0.001$) increased levels of cellular ^{59}Fe release at both 2.5 and 25 μM relative to the control, resulting in the mobilization of 29.4% and 29.9% of cellular ^{59}Fe, respectively (Fig. 5A). Notably, Ap44mSe was significantly ($p < 0.001$) more effective than DFO at releasing cellular ^{59}Fe at both 2.5 and 25 μM (Fig. 5A). At a concentration of 2.5 μM, Ap44mSe was slightly, but significantly ($p < 0.01$-0.05), less effective than Dp44mT or Ap44mT in terms of ^{59}Fe mobilization efficacy, but was comparable ($p > 0.05$) to Dp44mT and Ap44mT at 25 μM (Fig. 5A). These results demonstrate the similar activity of Ap44mSe relative to Dp44mT and Ap44mT in mediating ^{59}Fe mobilization from prelabeled cells, which could play a role in its high anti-proliferative efficacy.

Ap44mSe Demonstrates Marked Efficacy at Inhibiting Cellular ^{59}Fe Uptake from ^{59}Fe-Transferrin that is Much Greater than DFO and Similar to Dp44mT and Ap44mT

The ability of Ap44mSe to inhibit the cellular uptake of ^{59}Fe from the physiological Fe transport protein, transferrin (Tf), by SK-N-MC neuroepithelioma cells was also assessed and compared to the control ligands, DFO, Dp44mT and Ap44mT (Fig. 5B). This activity was examined as inhibiting cancer cell proliferation by targeting Fe by ligands involves not only increasing cellular Fe mobilization form cells, but also the prevention of cellular Fe uptake from Tf.[42]

As previously observed,[15,40] DFO demonstrated poor ability to inhibit the cellular uptake of ^{59}Fe from $^{59}Fe_2$-Tf, decreasing internalized ^{59}Fe uptake to 97.7% and 95.1% of the control at concentrations of 2.5 and 25 μM, respectively (Fig. 5B). At 2.5 μM, DFO showed comparable ability to inhibit cellular ^{59}Fe uptake relative to the control medium, but demonstrated significantly ($p < 0.05$) greater efficacy at 25 μM (Fig. 5B). In contrast, Dp44mT was able to markedly and significantly ($p < 0.001$) inhibit cellular ^{59}Fe uptake from $^{59}Fe_2$-Tf, decreasing it to 20.0% and 6.0% of the control at 2.5 and 25 μM, respectively (Fig. 5B). Similarly, Ap44mT significantly ($p < 0.001$)

inhibited ^{59}Fe uptake from $^{59}Fe_2$-Tf, to 14.5% and 6.6% of the control at 2.5 and 25 μM, respectively (Fig. 5B). Both Dp44mT and Ap44mT were significantly ($p < 0.001$) more effective at inhibiting cellular ^{59}Fe uptake from $^{59}Fe_2$-Tf relative to DFO at 2.5 and 25 μM.[15,40]

The selenosemicarbazone, Ap44mSe, significantly ($p < 0.001$) reduced ^{59}Fe uptake from $^{59}Fe_2$-Tf to 28.5% of the control at 2.5 μM, but was significantly ($p < 0.01$) less effective than Ap44mT at this concentration (Fig. 5B). Additionally, at 25 μM, Ap44mSe markedly reduced ^{59}Fe uptake to 8.7% of the control and was comparable in efficacy to its thiosemicarbazone counterparts, Dp44mT and Ap44mT (Fig. 5B). On the other hand, Ap44mSe was significantly ($p < 0.001$) more effective than DFO at inhibiting ^{59}Fe uptake at both 2.5 and 25 μM. Although Ap44mSe was not as effective at inhibiting cellular ^{59}Fe uptake relative to Ap44mT, these results indicate that its ability to inhibit Fe uptake from Tf could still play a significant role in the anti-proliferative activity of Ap44mSe.

Ap44mSe Alters the Expression of the Classical Iron-Regulated Genes, Transferrin Receptor-1 and Ferritin, and Up-Regulates the Metastasis Suppressor Protein, NDRG1

To determine whether the ability of Ap44mSe to chelate Fe, as observed through the ^{59}Fe efflux (Fig. 5A) and ^{59}Fe uptake (Fig. 5B) studies above, was involved in its anti-cancer activity, we further investigated if Ap44mSe could alter the expression of crucial proteins that are regulated by cellular Fe levels. The ability of Ap44mSe (10 μM) to alter the expression of the Fe uptake protein, transferrin receptor-1 (TfR1), and the Fe storage protein, ferritin,[44] was examined in comparison with DFO (100 μM), Dp44mT (10 μM) and Ap44mT (10 μM) after a 24 h/37°C incubation using SK-N-MC neuroepithelioma and SK-Mel-28 melanoma cells (Fig. 6). Notably, these ligand concentrations were utilized considering the low Fe chelation efficacy of DFO observed previously[45] and herein (Fig. 5A, B) relative to the marked activity of Dp44mT,[43] Ap44mT[15] and Ap44mSe (Fig. 5A, B). Furthermore, these cell-types were used as their Fe metabolism is well characterized and their response to chelators, such as DFO *etc.*, is well known.[42,46,47] The expression

of the metastasis suppressor, NDRG1, was also assessed upon incubation with Ap44mSe relative to DFO, Dp44mT and Ap44mT, due its pronounced regulation by cellular Fe levels *via* hypoxia-inducible factor-1α-dependent and independent mechanisms[23,48] and its potential as a promising therapeutic target against cancer.[21,22]

As previously demonstrated,[21,25] incubation with either DFO (100 μM) or Dp44mT (10 μM) significantly (p < 0.01-0.05) increased the expression of TfR1 in both SK-N-MC and SK-Mel-28 cells relative to the control (Fig. 6A,B), further indicating that these agents were able to sequester cellular Fe.[2,49] Similarly, Ap44mT and Ap44mSe also significantly (p < 0.01-0.05) increased the levels of TfR1 expression relative to the control in both cell-types, resulting in a 2.9- to 3.7-fold increase in TfR1 expression (Fig. 6A,B). The Ap44mSe-mediated increase in TfR1 expression was comparable to that observed with DFO, Dp44mT and Ap44mT in both SK-N-MC and SK-Mel-28 cells. The up-regulation of TfR1 expression by all chelators examined herein demonstrates the well known response of cells to Fe depletion.[44]

In contrast to TfR1 up-regulation, ferritin expression was down-regulated following incubation with the chelators (Fig. 6A, B). In these studies, ferritin in SK-N-MC cell lysates was resolved into its component H- and L- chains (Fig. 6A), while this was not apparent in SK-Mel-28 cells where ferritin migrated as a single band (Fig. 6B). The ligands, DFO, Dp44mT and Ap44mT mediated a significant (p < 0.001-0.01) decrease in ferritin expression in both SK-N-MC and SK-Mel-28 cells (Fig. 6A,B), resulting in a 1.7- to 8.3-fold decrease in ferritin expression. Incubation with Ap44mSe also induced a significant (p < 0.001-0.01) decrease in ferritin expression relative to the control, namely a 2.5- to 4.3-fold decrease in ferritin levels in SK-N-MC and SK-Mel-28 cells, respectively (Fig. 6A, B). This decrease in ferritin expression observed for all ligands examined herein indicates the classical response to cellular Fe depletion, where less ferritin is expressed due to the decreased need for Fe storage.[44]

Assessing NDRG1, multiple bands were observed in both cell-types (Fig. 6A, B), as reported previously in a variety of tumor cells.[45,50,51] These bands are thought to represent different cleavage forms or phosphorylation states of this protein.[21,52] Thus, the densitometry represents the total sum of all bands. The expression of NDRG1 was significantly ($p < 0.05$) increased upon DFO incubation in SK-N-MC cells and represented a 3-fold increase in NDRG1 expression (Fig. 6A). Levels of NDRG1 were also slightly, but not significantly ($p > 0.05$), increased upon incubation with DFO in SK-Mel-28 cells (Fig. 6B). As previously observed,[21,53] Dp44mT, markedly and significantly ($p < 0.001$-0.01) increased NDRG1 levels in both cell-types, resulting in a 11.6- to 33.9-fold increase in expression (Fig. 6A, B). In fact, Dp44mT was the most effective of the chelators examined at inducing NDRG1 expression. These results are in agreement with the ability of Dp44mT to increase the expression of Fe-regulated genes, such as *NDRG1* and *TfR1*, in tumor tissue upon *in vivo* administration.[13] Additionally, Ap44mT also significantly ($p < 0.001$-0.01) increased NDRG1 expression by 4.5- and 16.8-fold in SK-N-MC and SK-Mel-28 cells, respectively (Fig. 6A, B). Similarly, the selenosemicarbazone, Ap44mSe, also significantly ($p < 0.01$) increased NDRG1 levels in both cell-types relative to the control, representing a 5.5- to 12.7-fold increase in NDRG1 expression that was comparable to its thiosemicarbazone counterpart, Ap44mT (Fig. 6). In fact, the increase in NDRG1 levels mediated by Ap44mSe was significantly ($p < 0.01$-0.05) greater than that of DFO in both cell-types.

Considering that NDRG1 potently inhibits metastasis in multiple tumor-types,[54-56] and that metastasis kills 90% of cancer patients,[57] this property of Ap44mSe is important in terms of its potential efficacy as an anti-metastasis/tumor agent.

Ascorbate Oxidation Studies: Ap44mSe-Fe Complex Does Not Oxidize Ascorbate

In order to determine whether redox cycling played a role in the anti-proliferative activity of Ap44mSe, the ability of its Fe complex to mediate the oxidation of a physiological substrate,

ascorbate, was assessed (Fig. 7A). Notably, in these studies the Ap44mSe Cu complex was not assessed due to its low $Cu^{II/I}$ redox potential (Fig. 3) that does not facilitate the oxidation of ascorbate and this was confirmed by preliminary studies in this investigation. However, the redox activity of both the Cu and Fe complexes of Ap44mSe relative to Dp44mT and Ap44mT were assessed using an alternative method below (Fig. 7B).

The oxidation of ascorbate catalyzed by the Ap44mSe Fe complex was assessed in comparison to its parent Ap44mT counterpart (Fig. 7A). Both Dp44mT and EDTA were included as positive controls to accelerate ascorbate oxidation as shown previously,[15,39,40] while DFO acted as a negative control as its Fe complex inhibits ascorbate oxidation.[15,40] The results in the ascorbate oxidation assays are represented as Fe-binding equivalents (IBE) due to the different denticity of the chelators examined (*i.e.*, EDTA and DFO form 1:1 Fe/ligand complexes and are hexadentate, while Ap44mSe, Ap44mT and Dp44mT form 1:2 Fe/ligand complexes and bind in a tridentate manner). Three IBEs were examined, namely 0.1, 1, and 3, to assess the redox activity of their Fe complexes. An IBE of 0.1 corresponds to an excess of Fe to chelator, while an IBE of 1 represents a completely filled coordination sphere (*i.e.*, the formation of a 1:1 EDTA Fe complex or a 2:1 tridentate Fe complex). On the other hand, an IBE of 3 represents an excess of chelator relative to Fe.

In agreement with previous studies,[15,39,40] the Fe complex of EDTA demonstrated the greatest ability to mediate ascorbate oxidation, increasing it to 476% and 487% of the control at IBEs of 1 and 3, respectively (Fig. 7A). In contrast, the DFO-Fe complex acted in a protective manner, markedly inhibiting ascorbate oxidation to 43% and 21% of the control at IBEs of 1 and 3, respectively (Fig. 7A). The Fe complex of Dp44mT increased ascorbate oxidation to 251% and 177% of the control at IBEs of 1 and 3, respectively (Fig. 7A), as shown in previous studies.[15,39,40] Although the Fe complex of Dp44mT demonstrated significantly ($p < 0.01$) decreased levels of ascorbate oxidation relative to the Fe-EDTA complex, it showed significantly ($p < 0.001$) greater ability to mediate ascorbate oxidation compared to Fe-DFO at IBEs of 1 and 3.

In contrast, the Fe complex of Ap44mT did not effectively catalyze the oxidation of ascorbate due to its low $Fe^{III/II}$ redox potential (+49 *vs*. NHE)[15] that lies within a similar region to the two-electron ascorbate/dehydroascorbate couple (+60 mV *vs*. NHE).[58] Thus, there is little electrochemical driving force to enable the reaction. In fact, the Ap44mT-Fe complex resulted in 102% and 88% of ascorbate oxidation at IBEs of 1 and 3, respectively, and thus, was comparable to the control (Fig. 7A).

Additionally, the Fe complex of Ap44mSe mediated similar levels of ascorbate oxidation to that observed with the Fe complex of Ap44mT, catalyzing 109% and 92% of ascorbate oxidation relative to the control at IBEs of 1 and 3, respectively (Fig. 7A). The levels of ascorbate oxidation catalyzed by Fe complex of Ap44mSe were similar to both the control and the Fe complex of Ap44mT. This suggests that, like the Fe complex of Ap44mT, the $Fe^{III/II}$ redox potential of the Fe complex of Ap44mSe may be too low to effectively mediate ascorbate oxidation.

Cu Complexation by Ap44mSe, but not Fe, Induces Cellular ROS Generation

To further investigate the ability of Ap44mSe to form redox active Fe and Cu complexes, we examined their ability to catalyze the oxidation of the non-fluorescent molecule, 2',7'-dichlorodihydrofluorescein diacetate (H_2DCF-DA), to its fluorescent counterpart, dichlorofluorescein (DCF), in SK-N-MC cells (Fig. 7B). Notably, DCF is a widely used probe to examine levels of intracellular redox stress.[43,59,60] In these studies, hydrogen peroxide (H_2O_2; 50 µM), Ap44mT and Dp44mT were used as positive controls, as their ability to increase cellular ROS has been previously documented.[18,43]

To examine the ability of Ap44mSe to generate ROS, SK-N-MC cells were incubated with the chelators (2.5 µM alone or in the presence of Fe or Cu) for 30 min/37^{o}C, with or without a 15 min/37^{o}C pre-incubation with $FeCl_3$ (1.25 µM; 2:1) or $CuCl_2$ (2.5 µM; 1:1) and/or the non-toxic Cu

chelator, tetrathiomolybdate (TM; 5 μM). In these studies, TM was used as it is known to remove Cu from thiosemicarbazone-Cu complexes and prevent their redox activity.[18,19] The results were quantified by flow cytometry and are expressed as a percentage of the control (Fig. 7B).

Incubation of cells with the positive control, H_2O_2, led to a significant ($p < 0.001$) increase in H_2DCF oxidation to 133.1 ± 5.9% of control (Fig. 7B). In contrast, incubation of cells with $FeCl_3$, $CuCl_2$, or TM alone did not increase H_2DCF oxidation relative to control cells (Fig. 7B). The incubation of cells with Dp44mT, Ap44mT, or Ap44mSe alone did not significantly ($p > 0.05$) increase H_2DCF oxidation relative to control cells. The pre-incubation of cells with $FeCl_3$ followed by the addition of Dp44mT, Ap44mT, or Ap44mSe also had no significant ($p > 0.05$) effect on H_2DCF oxidation relative to control cells (Fig. 7B).

In contrast, the pre-incubation of cells with $CuCl_2$ followed by the addition of Dp44mT, Ap44mT, or Ap44mSe mediated a significant ($p < 0.001$) increase in intracellular H_2DCF oxidation to 218%, 170% and 164% of the control, respectively (Fig. 7B). In the presence of $CuCl_2$, Ap44mSe mediated significantly ($p < 0.05$) decreased H_2DCF oxidation relative to Dp44mT, but it was comparable to the thiosemicarbazone counterpart, Ap44mT (Fig. 7B). Pre-incubation of cells with TM and $CuCl_2$ followed by the addition of Dp44mT, Ap44mT, or Ap44mSe resulted in a significant ($p < 0.001$-0.01) decrease in H_2DCF oxidation to 103%, 98% and 98%, respectively, relative to cells incubated with $CuCl_2$ and Dp44mT, Ap44mT, or Ap44mSe (Fig. 7B).

Collectively, these results demonstrate the ability of the Cu complex of Ap44mSe to catalyze the formation of intracellular ROS. Significantly, the Cu chelator, TM, was able to attenuate this effect and highlights the importance of Cu chelation in the ability of Ap44mSe to catalyze ROS formation.

Ap44mSe Prevents Methemoglobin Formation

In the design of novel anti-cancer agents, the development of drugs that specifically target cancer cells with minimal side effects to normal cells is essential. Notably, methemoglobinemia and hypoxia are problematic side effects associated with the administration of 3-aminopyridine-2-carboxaldehyde thiosemicarbazone (3-AP; Triapine®), that has entered >20 phase I and II clinical trials.[61-65] Thus, it is critical to avoid these detrimental effects when designing novel thiosemicarbazone anti-cancer agents.

We previously demonstrated that the ability of 3-AP and Dp44mT to form redox active Fe complexes is vital in the formation of methemoglobin (metHb), an oxidation product of oxyhemoglobin (oxyHb) that cannot bind oxygen.[62] Thus, it was crucial to assess the ability of Ap44mSe to mediate metHb formation as this may provide an insight into its tolerability *in vivo*. In this study, the ability of Ap44mSe and its Cu and Fe complexes (25 μM) to catalyze metHb generation was examined in intact red blood cells (RBCs) after a 3 h incubation at 37°C and metHb formation was assessed by standard methods (Fig. 8).[62] This experiment was carried out in comparison to the control chelators, DFO, Dp44mT and Ap44mT and their Cu and Fe complexes (25 μM), as their ability to catalyze the formation of metHb has been previously characterized.[62]

As expected, metHb levels present in control RBCs and RBCs incubated with $FeCl_3$ alone were low, representing 0.25% and 0.20% of total Hb, respectively (Fig. 8). Additionally, RBCs incubated with $CuCl_2$ alone demonstrated a small, but significant ($p < 0.05$), increase in metHb levels representing 1.1% of total Hb (Fig. 8). As previously observed,[62] DFO and its Fe and Cu complexes did not significantly ($p > 0.05$) increase oxyHb oxidation relative to the control (Fig. 8).

In contrast, Dp44mT and its Fe and Cu complexes were able to significantly ($p < 0.01$-0.001) increase oxyHb oxidation relative to the control, resulting in a 71-, 191- and 78-fold increase in

metHb levels, respectively (Fig. 8). Importantly, the Fe complex significantly ($p < 0.001$) increased the generation of metHb relative to the ligand alone, as previously demonstrated.[62] On the other hand, the Cu complex of Dp44mT did not potentiate metHb formation and was comparable to the ligand alone (Fig. 8). As the Cu complexes of these ligands do not have the appropriate redox potential to oxidize oxyHb,[17,18] these results could suggest that transmetallation occurs, whereby the Cu complex donates Cu to the cell, releasing the ligand which then binds intracellular Fe which then acts to oxidize oxyHb. Notably, the mechanism of transmetallation by this general class of ligands is known.[17]

Ap44mT and its Fe and Cu complexes also significantly ($p < 0.001$-0.05) increased the levels of oxyHb oxidation compared to the control to 2.0%, 11.2% and 2.1%, respectively. As observed for Dp44mT, the addition of Fe significantly ($p < 0.01$) increased the ability of Ap44mT to catalyze oxyHb oxidation, while the addition of Cu did not promote metHb generation and was comparable to Ap44mT alone (Fig. 8). Importantly, the ability of Ap44mT and its Fe and Cu complexes to mediate oxyHb oxidation was significantly ($p < 0.001$-0.01) decreased relative to the corresponding Dp44mT ligand or its Fe and Cu complexes (Fig. 8).

Interestingly, the levels of metHb catalyzed by Ap44mSe or its Cu complex were found to be comparable to the control and were significantly ($p < 0.01$) less than Dp44mT or its Cu complex, respectively (Fig. 8). Although the Ap44mSe Fe complex was significantly ($p < 0.01$) more active at oxidizing oxyHb than the control, it was significantly ($p < 0.001$) less potent than the Dp44mT Fe complex (Fig. 8), and less effective ($p > 0.05$) than the Ap44mT-Fe complex. The differences in the ability of Dp44mT and Ap44mSe to catalyze metHb formation may be due to differences in ***(1)*** their lipophilicity, which would affect their ability to gain access to intracellular oxyHb; or ***(2)*** their ability to interact directly with and oxidize oxyHb.

In summary, unlike Dp44mT and Ap44mT, the ligand, Ap44mSe mediated decreased levels of oxyHb oxidation that was comparable to the control. This property highlights the potential tolerability of Ap44mSe *in vivo* and its clinical usefulness relative to either Dp44mT or Ap44mT.

The Ap44mSe-Cu Complex Targets Lysosomal Integrity

Previous work in our laboratory revealed that the lysosome is an important cellular target in the anti-cancer activity of the Cu thiosemicarbazone complex, Cu^{II}(Dp44mT).[19] The redox active Cu^{II}(Dp44mT) complex was found to accumulate in lysosomes, inducing cellular apoptosis by disruption of lysosomal integrity.[19] Due to the structural similarities between Ap44mSe, Ap44mT and Dp44mT (Fig. 1) and their ability to form redox active Cu complexes (Fig. 7B), we examined whether Ap44mSe also targets the lysosome using the lysosomotropic fluorophore, acridine orange (AO; Fig. 9A). The lysosomotropic agent, AO, is well known to accumulate in intact lysosomes to give a red punctate fluorescence, but it exhibits a diffuse green fluorescence upon redistribution to the cytosol or nucleus after lysosomal membrane permeabilization (LMP).[19,66,67]

To examine the ability of Ap44mSe, relative to its thiosemicarbazone counterparts, Ap44mT and Dp44mT, to affect lysosomal membrane integrity and AO localization, SK-N-MC cells were incubated with the chelators (2.5 μM) for 30 min/37˚C, with or without a 15 min/37˚C pre-incubation with $FeCl_3$ (1.25 μM; 1:2 complex) or $CuCl_2$ (2.5 μM; 1:1 complex). These cells were additionally pre-incubated with either: **(1)** control medium alone, or medium containing the glutathione (GSH) synthesis inhibitor, buthionine sulfoximine (BSO; 100 μM), for 16 h/37˚C; or **(2)** control medium alone or medium containing the anti-oxidant, *N*-acetyl-L-cysteine (NAC; 5 mM), for 15 min/37˚C; or **(3)** control medium alone, or medium containing the non-toxic Cu chelator, TM (5 μM), for 15 min/37˚C. Notably, BSO is known to enhance oxidative stress induced by Dp44mT by decreasing cellular levels of GSH through the inhibition of γ-glutamylcysteine synthetase.[19,68] In contrast, the anti-oxidant and GSH precursor, NAC,[69] has been demonstrated to

prevent the redox stress-mediated cytotoxicity of Dp44mT and its Cu complex.[19] The red fluorescence intensity was quantified with the image processing and analysis software, ImageJ v1.48 (National Institutes of Health, MD, USA; Fig. 9B).

Upon examining control cells by fluorescence microscopy, a granular red fluorescence consistent with AO accumulation in intact lysosomes was observed (Fig. 9A(a)). No significant difference in red fluorescence was observed upon pre-incubation with either: $FeCl_3$, $CuCl_2$, BSO, NAC or TM (Fig. 9A(b-f), 9B) relative to the control (Fig. 9A(a)), suggesting that these pre-incubation conditions did not significantly ($p > 0.05$) affect lysosomal integrity. Upon incubation of the cells with Dp44mT, Ap44mT, or Ap44mSe alone, no significant ($p > 0.05$) effect was observed on red fluorescence (Fig. 9A(g),(o),(w), 9B) relative to the control. Similarly, the pre-incubation of cells with $FeCl_3$ followed by incubation with Dp44mT, Ap44mT or Ap44mSe had no significant ($p > 0.05$) effect on red fluorescence relative to the control (Fig. 9A(h),(p),(x), 9B). Furthermore, the pre-incubation of cells with BSO or NAC with $FeCl_3$ followed by incubation with Dp44mT, Ap44mT or Ap44mSe also had no significant ($p > 0.05$) effect on red fluorescence compared to the control (Fig. 9A(i-j),(q-r),(y-z), 9B).

In contrast, pre-incubation of cells with $CuCl_2$ (2.5 μM) followed by incubation with Dp44mT, Ap44mT or Ap44mSe resulted in a marked and significant ($p < 0.001$) decrease in red fluorescence to 14%, 27% and 34%, respectively, of the control (Fig. 9B). This was accompanied by disappearance of lysosomal red vesicles consistent and the simultaneous increase in cytosolic green fluorescence consistent with the redistribution of AO to the cytosol,[19,66,67] indicating lysosomal damage (Fig. 9A(k),(s),(aa)). Notably, Dp44mT mediated the greatest reduction in red fluorescence in the presence of $CuCl_2$ and was significantly ($p < 0.001$-0.01) more effective in decreasing red AO fluorescence than either Ap44mT or Ap44mSe in the presence of $CuCl_2$ (Fig. 9B).

Furthermore, pre-incubation with BSO prior to the addition of $CuCl_2$ and the chelators, Dp44mT, Ap44mT, or Ap44mSe, led to a significant ($p < 0.001$) decrease of visible red fluorescence to 26%, 17% and 28%, respectively, relative to the control (Fig. 9A(l),(t),(ab), 9B). In fact, BSO significantly ($p < 0.01$-0.05) potentiated the ability of Ap44mT or Ap44mSe co-incubated with $CuCl_2$ to decrease red AO fluorescence relative to Ap44mT or Ap44mSe and $CuCl_2$ co-incubation alone (Fig. 9B). This observation suggested that the BSO-mediated depletion of GSH sensitized these cells to LMP by Ap44mT or Ap44mSe in the presence of $CuCl_2$.

Importantly, pre-incubation of cells with NAC or TM prior to the addition of $CuCl_2$ and either Dp44mT, Ap44mT, or Ap44mSe, successfully inhibited the relocation of AO from the lysosome to the cytosol (Fig. 9A(m-n),(u -v),(ac-ad)). Indeed, this NAC or TM pre-incubation significantly ($p < 0.001$) increased red fluorescence relative to cells incubated with $CuCl_2$ and the chelators alone (Fig. 9B). Furthermore, pre-incubation with TM or NAC prior to the addition of $CuCl_2$ and either Dp44mT, Ap44mT, or Ap44mSe resulted in levels of red fluorescence that were comparable to the control (Fig. 9B). Hence, both the anti-oxidant, NAC, and the Cu chelator, TM, decreased the pronounced ability of the chelators in the presence of $CuCl_2$ to mediate lysosomal damage, demonstrating the importance of both ROS generation and Cu chelation, respectively, in their ability to induce LMP.

Collectively, these results in Fig. 9 demonstrate that like Dp44mT and Ap44mT, the selenosemicarbazone, Ap44mSe, can mediate LMP in SK-N-MC cells *via* its Cu complex. This effect was potentiated upon pre-incubation with BSO that mediates the depletion of cellular GSH.[19,68] Moreover, both the anti-oxidant and GSH precursor, NAC,[69] and the Cu chelator, TM, could prevent Cu-Ap44mSe induced LMP. This AO study (Fig. 9), together with the DCF fluorescence data (Fig. 7B), suggests that Ap44mSe can form redox active Cu complexes that can mediate LMP.

The Copper Complex of Ap44mSe Mediates LMP and the Redistribution of Cathepsin D to the Cytosol

To further investigate the effect of Ap44mSe on the lysosome, we examined the ability of Ap44mSe and its Cu complex to alter the intracellular distribution and co-localization of the lysosomal membrane glycoprotein, lysosome-associated membrane protein 2 (Lamp2), with the soluble lysosomal enzyme, cathepsin D,[27,28] in SK-N-MC cells (Fig. 10). Upon damage to the lysosomal membrane, soluble enzymes present in the lysosomal lumen, such as cathepsin D, are released into the cytosol to trigger apoptotic signaling pathways.[27] Thus, the release of cathepsin D into the cytosol upon LMP leads to its decreased co-localization with the lysosomal membrane protein, Lamp2, and is a suitable marker to examine LMP.[14]

In these studies, SK-N-MC cells were successively incubated in 3 steps: ***(1)*** for 16 h/37˚C with either medium alone (control), or medium containing BSO (100 μM); or alternatively, for 15 min/37˚C with either medium alone (control) or medium containing NAC (5 mM) or TM (5 μM); ***(2)*** for 15 min/37˚C with either medium alone or medium containing $CuCl_2$ (2.5 μM); or ***(3)*** with medium alone or medium containing Ap44mSe (2.5 μM) for 30 min/37˚C. The effect of $FeCl_3$ in the presence of Ap44mSe on LMP was not further investigated in this study as no change in lysosomal integrity was observed upon co-incubation of $FeCl_3$ with Ap44mSe in the AO experiments (Fig. 9). The cells were then examined by immunofluorescence microscopy to assess the co-localization of cathepsin D (green; Fig. 10A) and Lamp2 (red; Fig. 10A). Nuclei were stained blue with 4',6-diamidino-2-phenylindole (DAPI; Fig. 10A(a,e,i,m,q,u,y)). The levels of green fluorescence due to cathepsin D were quantified with the image processing and analysis software, ImageJ v1.48 (Fig. 10B).

Control SK-N-MC cells stained for Lamp2 and cathepsin D demonstrated a vesicular pattern consistent with that of lysosomes (Fig. 10A(b-c)). Significantly, upon overlaying the Lamp2 (Fig.

10A(b)) and cathepsin D (Fig. 10A(c)) images, a yellow granular pattern was observed, demonstrating their co-localization in intact lysosomes (Fig. 10A(d)). Similarly, pre-incubation with $CuCl_2$ alone did not significantly ($p > 0.05$) alter cathepsin D and Lamp2 localization, with a yellow punctate vesicular pattern being observed ((Fig. 10A(h)), suggesting intact lysosomes. Additionally, there was no significant ($p > 0.05$) change in cathepsin D green fluorescence upon $CuCl_2$ incubation relative to the control (Fig. 10B). In agreement with the AO results (Fig. 9), Ap44mSe alone did not significantly ($p > 0.05$) affect the integrity of the lysosomal membrane, resulting in a similar yellow punctate pattern (Fig. 10A(l)) and comparable levels of green fluorescence relative to the control (Fig. 10A(d), 10B).

Conversely, the pre-incubation of cells with $CuCl_2$ followed by Ap44mSe resulted in a marked alteration in the morphology of Lamp2 (Fig. 10A(n)) and cathepsin D (Fig. 10A(o)) staining with a distinct loss of yellow punctate structures in the overlay (Fig. 10A(p)) relative to the control (Fig. 10A(d)). In fact, under the latter condition, a significant ($p < 0.001$) loss of green cathepsin D fluorescence (Fig. 10A(o)) was observed upon $CuCl_2$ and Ap44mSe incubation, resulting in a decrease to 24% of the control value (Fig. 10B). This collectively suggested the redistribution of cathepsin D from the lysosome into the cytosol after LMP. These observations are consistent with our AO studies above (Fig. 9) and suggest that co-incubation of Ap44mSe and $CuCl_2$ impairs lysosomal integrity.

Additionally, pre-incubation of cells with the GSH synthesis inhibitor, BSO, prior to $CuCl_2$ and Ap44mSe incubation, also demonstrated a marked decrease in the punctate staining of both Lamp2 (Fig. 10A(r)) and especially cathepsin D (Fig. 10A(s)) relative to the respective Controls (Fig. 10A(b), (c)). This effect resulted in a pronounced reduction in the co-localization of these proteins, evident by reduced yellow fluorescence in the overlay (Fig. 10A(t)) compared to the control (Fig.

10A(d)). Moreover, a significant ($p < 0.001$) decrease in green cathepsin D fluorescence was observed (Fig. 10B).

In contrast, pre-incubation of cells with the anti-oxidant, NAC, or the Cu chelator, TM, prior to $CuCl_2$ and Ap44mSe incubation, restored the punctate staining of Lamp2 (Fig. 10A(v)(z)) and cathepsin D (Fig. 10A(w)(aa)) relative to the $CuCl_2$ and Ap44mSe incubation alone (Fig. 10A(n),(o)). Moreover, in the overlay of Lamp2 and cathepsin D, the yellow vesicular pattern consistent with intact lysosomes was maintained upon pre-incubation with NAC (Fig. 10A(x)) or TM (Fig. 10A(ab)) prior to $CuCl_2$ and Ap44mSe incubation. In fact, the pre-incubation with NAC or TM prior to treatment with $CuCl_2$ and Ap44mSe, resulted in levels of green cathepsin D fluorescence that were significantly ($p < 0.001$) increased to 89% or 90% of the control, respectively, relative to when the incubation was performed with $CuCl_2$ and Ap44mSe alone (24%; Fig. 10B). These results were in agreement with the AO experiments (Fig. 9) that demonstrated the ability of both NAC and TM to prevent $CuCl_2$- and Ap44mSe-mediated damage to lysosomes.

In conclusion, these results in Figs 7B, 9 and 10 demonstrate that Ap44mSe can form redox active Cu complexes which generate ROS and target lysosomal membrane integrity to induce LMP. This effect was prevented by the chelation of Cu by TM, or the supplementation of cellular GSH *via* NAC, suggesting that the formation of a redox active Cu-Ap44mSe complex was vital in the induction of LMP.

Conclusions

Selenosemicarbazones have gained considerable attention due to their activity as anti-bacterial, anti-parasitic, anti-viral and anti-cancer agents.[30-38] Significantly, selenosemicarbazones and their metal complexes have been observed to exhibit potent anti-cancer activity both *in vitro*[30-34] and *in vivo* with high tolerability.[30,31] Despite extensive investigations on the biological activity of selenosemicarbazones, further studies were required to elucidate their cellular targets and mechanisms of action. In this investigation, we compared the selectivity and mechanisms of action of the selenosemicarbazone, Ap44mSe, in comparison to its well characterized thiosemicarbazone counterparts, Ap44mT and Dp44mT.

Notably, an important structure-activity relationship derived from this study is that the substitution of chalcogen S atom in the thiocarbonyl moiety with selenium did not markedly affect anti-proliferative activity, but led to a marked 3-4-fold increase in the selective anti-tumor activity (*i.e.*, therapeutic index) against cancer cells relative to normal mortal cells. This represents a marked improvement in efficacy, as a major problem with current anti-tumor chemotherapy is that it suffers from non-specific side effects against normal tissue. Hence, future chemotherapeutic design of thiosemicarbazones, particularly the highly potent second generation of di-2-pyridylketone thiosemicarbazones,[21,70] could implement selenium substitution of the thiocarbonyl group.

Another significant structure-activity relationship was that Ap44mSe relative to the parent ligand, Ap44mT, exhibited less metHb generation activity as the ligand, Fe complex and also Cu complex (Fig. 8). This is important, as metHb is a side effect observed upon the clinical administration of the thiosemicarbazone, 3-AP,[61,63,71,72] and is also observed after the *in vivo* administration of Dp44mT.[62] In fact, the metHb generation by the Ap44mSe was markedly and significantly less pronounced than that mediated by Dp44mT in erythrocytes (Fig. 8). As an additional appropriate clinically relevant property, Ap44mSe induced the up-regulation of the metastasis suppressor

protein, NDRG1, which has been shown to be important in suppressing the metastasis of a variety of aggressive tumors.[54,55,73] This property is vital, as metastasis results in the death of 90% of cancer patients,[57] and hence, agents that can effectively up-regulate NDRG1 as an important therapeutic target are essential to develop.[73] Of note, Ap44mSe was not as effective as Dp44mT in up-regulating NDRG1. However, its ability to achieve markedly higher anti-tumor selectivity and lower metHb generation than either Dp44mT or Ap44mT, means collectively, it has greater potential as an anti-cancer/anti-metastatic chemotherapeutic.

For the first time, the current study identified that Ap44mSe could target lysosomal integrity *via* the formation of redox active Cu complexes. Intracellular DCF studies demonstrated that Cu, but not Fe, complexes of Ap44mSe mediated significant levels of ROS generation that could be attenuated by the non-toxic Cu chelator, TM (Fig. 7B). Significantly, the Cu complex, but not the Fe complex, of Ap44mSe targeted the lysosome to induce LMP, as observed through both AO and cathepsin D fluorescence studies. Clearly, the formation of ROS and Cu complexation was critical for this effect, as both the anti-oxidant, NAC, and Cu chelator, TM, could prevent the Cu-Ap44mSe-mediated LMP. Importantly, the redistribution of cathepsin D from the lysosome to the cytosol following Cu-Ap44mSe-mediated LMP is a critical step in the initiation of apoptosis, and is an early event in the apoptotic cascade prior to mitochondrial destabilization.[28,29]

In conclusion, for the first time, we demonstrate the ability of Ap44mSe to form redox active Cu complexes that mediate ROS formation and target the lysosome to induce LMP. Hence, the ability of selenosemicarbazones to induce cytotoxicity *via* the lysosome represents an important therapeutic approach worthy of further examination. Moreover, the current study highlights the importance of the thiocarbonyl S to Se substitution in generating advantageous pharmacological properties and the therapeutic potential of Ap44mSe as an anti-cancer/anti-metastatic agent that limits metHb formation and displays a very high therapeutic index.

Experimental Procedures

Materials

All purchased reagents were of the highest purity available and utilized without additional purification. The Dp44mT, Ap44mT and Ap44mSe precursors, namely: di(2-pyridyl)ketone, 2-acetylpyridine, 4,4-dimethyl-3-thiosemicarbazide, selenium and sodium borohydrate, DFO, NAC and TM were obtained from Sigma-Aldrich (St. Louis, MO, USA). The chelators, Dp44mT and Ap44mT, were prepared and characterized *via* previously described methods.[15,40] Elemental analysis (C, H, N) of the synthesized ligands and complexes was performed by established methods[15,17,18,39,40] and determined the purity of the biologically examined compounds to be >95%.

Chemical Studies

Physical Methods

^{1}H NMR (400 MHz) spectra were acquired using a Bruker Avance 400 NMR spectrometer with DMSO-d_6 as the solvent and internal reference (Me_2SO: ^{1}H NMR δ 2.50 ppm and ^{13}C NMR δ 39.5 ppm *vs.* TMS). Infrared spectra were measured with a Varian Scimitar 800 FT-IR spectrophotometer with compounds dispersed as KBr discs.

Cyclic voltammetry was performed using a BAS100B/W potentiostat employing a glassy carbon working electrode, a Pt wire auxiliary electrode and an aqueous Ag/AgCl reference electrode. All complexes were at *ca.* 1 mM in MeCN:H_2O (70:30 v/v). This solvent combination was used to ensure the solubility of all compounds and allowed direct comparisons to previous studies using this solvent combination.[15,39,40] The supporting electrolyte was Et_4NClO_4 (0.1 M) and all solutions were purged with nitrogen prior to measurement. All potentials are cited *versus* the NHE by addition of 196 mV to the potentials measured relative to the Ag/AgCl reference electrode.

Electron paramagnetic resonance (EPR) spectra were measured on a Bruker ER200 instrument at X-band frequency (~9.3 GHz) in 1 mM DMF frozen solutions at 130 K. Spectra were simulated with the program EPR50F.[74] All simulated spectra and their spin Hamiltonian parameters appear in the Electronic Supporting Information.

Crystallography

Crystallographic data were acquired at 293 K on an Oxford Diffraction Gemini CCD diffractometer employing graphite-monochromated Mo-Kα radiation (0.71073 Å) and operating within the range $2 < 2\theta < 50$ Å. Data reduction and empirical absorption corrections (multi-scan) were performed with Oxford Diffraction CrysAlisPro software. Structures were solved by direct methods with SHELXS and refined by full-matrix least-squares analysis with SHELXL-97.[75] All non-H atoms were refined with anisotropic thermal parameters. Molecular structure diagrams were produced with ORTEP3.[76] The data in CIF format has been deposited at the Cambridge Crystallographic Data Centre (CCDC 1420429 and 1420430).

Syntheses

2-Acetylpyridine 4,4-dimethyl-3-selenosemicarbazone (Ap44mSe*)*

The ligand was synthesized following a published protocol,[38] with slight modifications. A suspension of 2-acetylpyridine 4,4-dimethyl-3-thiosemicarbazone (1 g, 4.5 mmol) in 10 mL of H_2O was treated with 5 mL of 50% w/w aqueous NaOH. The suspension was stirred vigorously for 10 min, followed by the dropwise addition of methyl iodide (0.78 g, 5.5 mmol) over 10 min. This turned the orange suspension to a yellow oil. The oil was extracted into 50 mL diethyl ether, which was then washed with H_2O (25 mL x 4) and brine (25 mL x 2), and dried with magnesium sulfate. The solvent was removed under vacuum. A solution of sodium hydrogen selenide was then prepared. This involved combining selenium (0.59 g, 7.5 mmol) with sodium borohydride (0.32 g, 8.5 mmol) in 25 mL of ethanol under argon. To this solution, the *S*-methyl precursor formed above

was added, dissolved in 15 mL of ethanol and stirred for 48 h. The product was poured into 40 mL of 10% (w/w) aqueous acetic acid and extracted into 50 mL of dichloromethane. This was then washed with H_2O (25 mL x 4) and dried over magnesium sulfate. The solvent was removed under vacuum and the product was recrystallized from dry ethanol, yielding fine orange needles (yield 0.43 g, 36%). Anal. Calc. for $C_{10}H_{14}N_4Se$: C, 44.6; H, 5.2; N, 20.8. Found: C, 44.5; H, 5.0; N, 20.5%. ^{1}H NMR (DMSO-d_6): δ 14.6 (s, 1H, NH), 8.7 (m, 1H, py), 8.0 (m, 1H, py), 7.8 (m, 1H, py), 7.5 (m, 1H, py), 3.3 (s, 6H, $N(CH_3)_2$), 2.6 (s, 3H, CCH_3).

[Cu(Ap44mSe)(OAc)]

The synthesis of this compound was based on the procedure employed for the thiosemicarbazone analogue, Ap44mT.[18] Ap44mSe (0.20 g, 0.74 mmol) was dissolved in DMF (10 mL) with stirring and gentle heating. A solution of $Cu(OAc)_2 \cdot H_2O$ (0.15 g, 0.75 mmol) in water (7 mL) was added gradually with stirring and the solution rapidly darkened. On standing, dark brown blocks of the product formed which were suitable for X-ray work. These were filtered off, washed with EtOH (5 mL) and diethyl ether (5 mL), and then dried in a vacuum desiccator (yield 0.11 g, 38%). Anal. Calcd. for $C_{12}H_{16}CuN_4O_2Se$: C, 36.9; H, 4.1; N, 14.3%. Found: C: 37.1; H: 4.1; N: 13.7%. IR $\bar{\nu}$ (cm^{-1}, all strong) 1608, 1516, 1399, 1370, 1313, 1258, 1106, 894, 774. Electronic spectrum (MeCN) λ_{max}, nm (ε, M^{-1} cm^{-1}): 425 (35,700), 348 (46,800), 308 (53,900).

$[Cu_2(Ap44mSe)_3](ClO_4) \cdot 3H_2O$

A solution of Ap44mSe (100 mg, 0.37 mmol) and Et_3N (37 mg, 0.37 mmol) in EtOH (5 mL) was gently warmed to dissolve the ligand. A solution of $Cu(ClO_4)_2 \cdot 6H_2O$ (69 mg, 0.19 mmol) was added with stirring and the mixture darkened immediately. The reaction mixture was refluxed for 30 min. On cooling, a dark brown precipitate formed which was filtered off, washed with EtOH and diethyl ether then dried in a vacuum desiccator (yield 46 mg, 22%). Anal. Calcd. for $C_{30}H_{45}ClCu_2N_{12}O_7Se_3$: C, 33.2; H, 4.2; N, 15.5%. Found: C, 33.2; H, 3.5; N, 15.3%. IR $\bar{\nu}$ (cm^{-1}, all

strong) 1505, 1391, 1299, 1248, 1078 (br), 891, 778. Electronic spectrum (MeCN) λ_{max}, nm (ε, M^{-1} cm^{-1}): 425 sh (22,300), 362 (47,800), 311 sh (37,200). Crystals of $[Cu_2(Ap44mSe)_3](ClO_4)\cdot THF$ suitable for X-ray work were grown by vapour diffusion of THF into a MeCN solution of the complex.

Biological Studies

Cell Culture

Chelators (Dp44mT, Ap44mT and Ap44mSe) were dissolved in DMSO as 10 mM stock solutions, which were subsequently diluted in medium containing 10% fetal calf serum (Life Technologies, CA, USA), resulting in a final [DMSO] < 0.5% (v/v). At this final concentration, DMSO had no effect on proliferation, ^{59}Fe uptake, or ^{59}Fe mobilization from cells, as shown previously.[42] DFO was directly dissolved as a 1 mM stock solution in culture medium. The human SK-N-MC neuroepithelioma, SK-Mel-28 melanoma and mortal human MRC5 fibroblast cells were obtained from American Type Culture Collection (Manassas, VA) and grown according to established procedures[42,43] in a humidified atmosphere of 5% CO_2 and 95% air at 37°C in an incubator (Forma Scientific, Marietta, OH).

Effect of the Chelators on Cellular Proliferation

The effect of the chelators and their Fe and Cu complexes on cellular proliferation were determined *via* the [1-(4,5-dimethylthiazol-2-yl)-2,5-diphenyl tetrazolium] (MTT) assay by standard methods.[39,40,42] Human SK-N-MC or MRC5 cells were seeded in 96-well microtiter plates at 1.5×10^4 or 1.0×10^4 cells/well, respectively, in medium containing human $^{56}Fe_2$-Tf (1.25 μM) and chelators or their Fe or Cu complexes at a range of concentrations (0-25 μM). The cells were incubated for 72 h/37°C in a humidified atmosphere containing 95% air and 5% CO_2, after which 10 μL of MTT (5 mg/mL) was added to each well and then incubated for 2 h/37°C. The cells were subsequently solubilized using 100 μL of 10% SDS-50% isobutanol in 10 mM HCl and the plates

were then read at 570 nm using a scanning multi-well spectrophotometer. The inhibitory concentration (IC_{50}) was defined as the chelator concentration required to decrease the absorbance to 50% of the untreated control.

Preparation of ^{56}Fe- and $^{59}Fe_2$-Transferrin

Human apo-Tf (Sigma-Aldrich) was labeled with ^{56}Fe or ^{59}Fe (PerkinElmer, MA, USA; 50-65 mCi/mg) to yield $^{56}Fe_2$-Tf or $^{59}Fe_2$-Tf (500 pCi/pmol Fe), respectively.[42,77] Any unbound ^{59}Fe was removed by passage through a Sephadex G25 column and exhaustive dialysis against an excess of 0.15 M NaCl at pH 7.4 by standard procedures.[42,77] ***Caution:*** ^{59}Fe is a β-emitter (0.273 MeV (45%); 0.466 (53%)) and γ-emitter (1.099 MeV (57%); 1.292 MeV (43%)). Primary Perspex shielding and secondary lead shielding are required to minimize exposure and to minimize the generation of Bremsstrahlung X-rays.

Effect of Chelators on ^{59}Fe Efflux from Cells

Experiments examining the ability of the chelators to mobilize ^{59}Fe from prelabeled SK-N-MC cells were performed according to established methods.[42,78] In these studies, Ap44mSe was compared to the previously characterized chelators, DFO, Dp44mT and Ap44mT. Cells were prelabeled using $^{59}Fe_2$-Tf (0.75 μM) for 3 h/37°C, washed on ice four times with ice-cold PBS and then subsequently incubated with each chelator (2.5 or 25 μM) for 3 h/37°C. The overlying media was then separated from the cells using a Pasteur pipette. Radioactivity was measured in both the cell pellet and supernatant using a *γ*-scintillation counter (Wallac Wizard 3, Turku, Finland).

Effect of Chelators at Preventing ^{59}Fe Uptake from $^{59}Fe_2$-Tf by Cells

The ability of the chelator to prevent cellular ^{59}Fe uptake from the serum Fe transport protein, $^{59}Fe_2$-Tf, was examined using well established techniques.[40,42] Cells were incubated with $^{59}Fe_2$-Tf (0.75 μM) for 3 h/37°C in the absence (control) or presence of the chelators (2.5 or 25 μM) and then

washed four times with ice-cold PBS. Internalized ^{59}Fe uptake was determined by incubating the cell monolayer for 30 min/4°C with the general protease, Pronase (1 mg/mL; Sigma-Aldrich).[40,42] The cells were removed from the monolayer using a plastic spatula and centrifuged at 14,000 rpm/1 min. The Pronase-insensitive fraction represented internalized ^{59}Fe, while the supernatant represented membrane-bound, Pronase-sensitive ^{59}Fe that was released by the protease.[40,42] Ap44mSe was compared to the previously characterized chelators, DFO, Dp44mT and Ap44mT that acted as controls.

Western Blotting

Western blotting was performed by standard methods, as previously described.[79] The following antibodies were used at a range of antibody concentrations as indicated by the manufacturers to probe for specific proteins: goat polyclonal anti-NDRG1 (Abcam; Cat. #: ab37897, 1/2,000), mouse monoclonal anti-human TfR1 (clone H68.4; Invitrogen; Cat. #: 136800, 1/1,000), rabbit monoclonal anti-ferritin (Abcam; Cat. #: ab75973, 1/1,000) and mouse monoclonal anti-β-actin (clone AC-40; Sigma-Aldrich; Cat. #: A4700, 1/10,000). The secondary antibodies used were: horseradish peroxidase-conjugated anti-goat (Sigma-Aldrich; Cat. #: A5420); anti-mouse (Sigma-Aldrich; Cat. #: A9044); and anti-rabbit (Sigma-Aldrich; Cat. #: A0545); and implemented at dilutions indicated by the manufacturers (1/5,000-1/20,000). Membranes were washed, developed and quantified using a ChemiDoc XRS Station (Bio-Rad). All data were normalized to the loading control, β-actin.

Ascorbate Oxidation Assay

The ability of the chelators to mediate the oxidation of ascorbate was examined using an established protocol.[40,80] Ascorbic acid (100 μM) was prepared immediately prior to the experiment and incubated in the presence of the chelator (1-60 μM), Fe^{III} (10 μM; as $FeCl_3$), in a 50-fold molar excess of citrate (500 μM) to prevent hydrolytic polymerization of Fe^{III}. The absorbance at 265 nm

was monitored after 10 and 40 min at room temperature. The difference in absorbance between these time points was then calculated.[15,40]

Intracellular ROS Measurements

Levels of intracellular ROS generation were measured using the H_2DCF-DA assay.[43,59] H_2DCF-DA is hydrolyzed by intracellular esterases to H_2DCF, which becomes trapped within the cytosol. Cellular oxidants oxidize non-fluorescent H_2DCF to the fluorescent product, DCF.[43,59] SK-N-MC cells were incubated with H_2DCF-DA (25 μM) for 30 min/37°C and then washed twice with ice-cold PBS. The cells were incubated with either the positive control, H_2O_2 (50 μM), or a chelator (2.5 μM) for 30 min/37°C. To examine the ability of Fe, Cu or Cu chelation to alter chelator-mediated H_2DCF oxidation, a 15 min/37°C pre-incubation of cells with $FeCl_3$ (1.25 μM), $CuCl_2$ (2.5 μM) and/or TM (5 μM) was used, respectively, prior to incubation of the cells with the chelators (2.5 μM). The cells were then collected for flow cytometric assessment. Intracellular ROS was detected as an increase in green cytosolic DCF fluorescence using a FACS Canto flow cytometer (Becton Dickinson, Lincoln Park, NJ, USA). In these experiments, 10,000 events were acquired for every sample and the data was analyzed using FlowJo software v7.5.5 (Tree Star Inc., Ashland, OR).

Hemoglobin Preparation and Spectral Analysis of MetHb

Hemoglobin samples were prepared as described previously.[62] Blood samples were collected from healthy human donors in Vacutainer® collection tubes (BD, Plymouth, UK) and used immediately. RBCs were isolated by centrifugation (480 x *g*/5 min/4ºC) and then washed in Hank's balanced salt solution (HBSS) and subsequently resuspended in this buffer.[62] Experiments implementing intact RBCs (15% hematocrit) were performed for 3 h/37ºC in the absence or presence of chelators or their Fe or Cu complexes (25 μM). Spectra (250-700 nm) of RBC lysates were obtained using a Shimadzu UV-Vis spectrophotometer (UV-1800; Shimadzu, Kyoto, Japan) and levels of metHb

were measured as previously described.[62] Concentrations of oxyHb and metHb were determined at 577 and 630 nm, respectively.[81]

Assessment of Lysosomal Membrane Permeability

The intracellular distribution of AO (Sigma-Aldrich) observed by fluorescence microscopy was used to assess LMP as previously described and was quantified using ImageJ v 1.48 software.[19] The cells were incubated for 12 min/37°C with AO (2.5 μM) and then washed once with FCS-free medium. Cells were incubated with the chelators (2.5 μM) for 30 min/37°C with or without a 15 min/37°C pre-incubation with $FeCl_3$ (1.25 μM) or $CuCl_2$ (2.5 μM).

To further examine the role of redox stress or Cu chelation in chelator-mediated LMP, cells were pre-incubated with: BSO (100 μM) for 16 h/37°C; or NAC (5 mM) or TM (5 μM) for 15 min/37°C prior to incubation with $FeCl_3$, $CuCl_2$ or the chelators. The cells were examined with a Zeiss Axio Observer.Z1 fluorescence microscope (Zeiss, Germany) that was equipped with Texas Red and FITC filters. Images were captured using an AxioCam camera and AxioVision Rel. 4.7 Software (Zeiss, Germany). Data analysis was performed using ImageJ v 1.48 software.

Immunofluorescence Studies of Lysosomal Membrane Permeabilization

Lysosomal permeability was examined with immunofluorescence by examining the release of the lysosomal protein, cathepsin D, as previously reported.[14,19] Lamp2 was used to examine co-localization with lysosomes as previously reported.[14] Cells were incubated with Ap44mSe (2.5 μM) for 30 min/37°C with or without a 15 min/37°C pre-incubation with $CuCl_2$ (2.5 μM). To further examine the role of redox stress or Cu chelation in LMP, cells were pre-incubated with: BSO (100 μM) for 16 h/37°C; or NAC (5 mM) or TM (5 μM) for 15 min/37°C prior to incubation with $CuCl_2$ or Ap44mSe. The fluorescence microscope and camera system detailed above was used to examine

green (excitation, 495 nm, emission, 516 nm) and red (excitation, 577 nm, emission, 592 nm) fluorescence. Green fluorescence was quantified using ImageJ v 1.48 software.

Statistical Analysis

Experimental data were compared using Student's *t*-test. Results were expressed as mean ± SD and considered to be statistically significant when $p < 0.05$.

Supporting Information Available: *Experimental and simulated EPR spectrum of [Cu(Ap44mSe)(OAc)]*. This material is available free of charge *via* the Internet at http://pubs.acs.org.

*__Authors for Correspondence:__ Prof. P.V. Bernhardt, Ph: +61-7-3365-4266; FAX +61-7-3365-4299; email: p.bernhardt@uq.edu.au; Dr D.S. Kalinowski, Ph: +61-2-9351-8976; FAX +61-2-9351-3429; Email: danutak@med.usyd.edu.au; Prof. D.R. Richardson, Ph: +61-2-9036-6548; FAX +61-2-9036-6549; Email: d.richardson@med.usyd.edu.au

Author Contributions: Z.A. performed studies, prepared figures and wrote the manuscript; C.S. A.A., P.C.S., M.T.B., N.K. and S.S. performed studies; P.J.J. designed studies; Z.K. and D.J.R.L. wrote the manuscript; D.R.R. designed studies and wrote the manuscript; P.V.B. and D.S.K. designed studies, prepared figures and wrote the manuscript. D.S.K. and D.R.R. participated as equal senior authors.

Acknowledgments

This work was supported by a Project Grant from the National Health and Medical Research Council (NHMRC) Australia to D.R.R. [1021607] and D.S.K. [1048972]; a NHMRC Senior Principal Research Fellowship to D.R.R. [1062607]; a NHMRC RD Wright Fellowship to D.S.K. [1083057]. P.J.J. (10/CDF/2-15) thanks the Cancer Institute NSW for Fellowship support. S.S. thanks the Sydney Medical School for an Early Career Research Grant. Z.K. sincerely appreciates an NHMRC Peter Doherty Early Career Fellowship [1037323] and Cancer Institute NSW Early Career Fellowship [12ECF2-17]. D.J.R.L. thanks the Sydney Medical School Foundation for Fellowship support and the AMP Tomorrow Fund for grant support. C.S. is the grateful recipient of an Australian Postgraduate Award from the University of Sydney. P.V.B. is grateful for a Discovery Grant (DP150104672) from the Australian Research Council.

Abbreviations

AO, acridine orange; Ap44mT, 2-acetylpyridine 4,4-dimethyl-3-thiosemicarbazone; Ap44mSe, 2-acetylpyridine 4,4-dimethyl-3-selenosemicarbazone; BSO, buthionine sulfoximine; DAPI, 4',6-diamidino-2-phenylindole; DCF, 2′,7′-dichlorofluorescein; DFO, desferrioxamine; Dp44mT, di-2-pyridylketone 4,4-dimethyl-3-thiosemicarbazone; GSH, glutathione; H_2DCF-DA, 2′,7′-dichlorodihydrofluorescein diacetate; H_2DCF, 2′,7′-dichlorodihydrofluorescein; IBE, iron-binding equivalent; Lamp2, lysosome-associated membrane protein 2; LMP, lysosomal membrane permeabilization; metHb, methemoglobin; MTT, 1-(4,5-dimethylthiazol-2-yl)-2,5-diphenyltetrazolium; NAC, *N*-acetyl-L-cysteine; NDRG1, *N*-myc downstream regulated gene-1; NHE, normal hydrogen electrode; oxyHb, oxyhemoglobin; PBS, phosphate buffered saline; RBC, red blood cell; ROS, reactive oxygen species; RR, ribonucleotide reductase; Tf, transferrin; TfR1, transferrin receptor-1; TM, tetrathiomolybdate; 3-AP, 3-aminopyridine-2-carboxaldehyde thiosemicarbazone.

References

1. Yu, Y.; Kalinowski, D. S.; Kovacevic, Z.; Siafakas, A. R.; Jansson, P. J.; Stefani, C.; Lovejoy, D. B.; Sharpe, P. C.; Bernhardt, P. V.; Richardson, D. R. Thiosemicarbazones from the old to new: Iron chelators that are more than just ribonucleotide reductase inhibitors. *J. Med. Chem.* **2009**, *52*, 5271-5294.

2. Kalinowski, D. S.; Richardson, D. R. The evolution of iron chelators for the treatment of iron overload disease and cancer. *Pharmacol. Rev.* **2005**, *57*, 547-583.

3. Yu, Y.; Wong, J.; Lovejoy, D. B.; Kalinowski, D. S.; Richardson, D. R. Chelators at the cancer coalface: desferrioxamine to Triapine and beyond. *Clin. Cancer Res.* **2006**, *12*, 6876-6883.

4. Torti, S. V.; Torti, F. M. Iron and cancer: More ore to be mined. *Nat. Rev. Cancer* **2013**, *13*, 342-355.

5. Nasulewicz, A.; Mazur, A.; Opolski, A. Role of copper in tumour angiogenesis—clinical implications. *J. Trace Elem. Med. Biol.* **2004**, *18*, 1-8.

6. Raju, K. S.; Alessandri, G.; Ziche, M.; Gullino, P. M. Ceruloplasmin, copper ions, and angiogenesis. *J. Natl. Cancer Inst.* **1982**, *69*, 1193-1188.

7. Xie, H.; Kang, Y. J. Role of copper in angiogenesis and its medicinal implications. *Curr. Med. Chem.* **2009**, *16*, 1304-1314.

8. Hassouneh, B.; Islam, M.; Nagel, T.; Pan, Q.; Merajver, S. D.; Teknos, T. N. Tetrathiomolybdate promotes tumor necrosis and prevents distant metastases by suppressing angiogenesis in head and neck cancer. *Mol. Cancer Ther.* **2007**, *6*, 1039-1045.

9. Huang, X. Iron overload and its association with cancer risk in humans: Evidence for iron as a carcinogenic metal. *Mutat. Res. Fund. Mol. M.* **2003**, *533*, 153-171.

10. Torti, S. V.; Torti, F. M.; Whitman, S. P.; Brechbiel, M. W.; Park, G.; Planalp, R. P. Tumor cell cytotoxicity of a novel metal chelator. *Blood* **1998**, *92*, 1384-1389.

11. Aouad, F.; Florence, A.; Zhang, Y.; Collins, F.; Henry, C.; Ward, R. J.; Crichton, R. R. Evaluation of new iron chelators and their therapeutic potential. *Inorg. Chimica Acta* **2002**, *339*, 470-480.

12. Richardson, D.; Ponka, P.; Baker, E. The effect of the iron(III) chelator, desferrioxamine, on iron and transferrin uptake by the human malignant melanoma cell. *Cancer Res.* **1994**, *54*, 685-689.

13. Whitnall, M.; Howard, J.; Ponka, P.; Richardson, D. R. A class of iron chelators with a wide spectrum of potent antitumor activity that overcomes resistance to chemotherapeutics. *Proc. Natl. Acad. Sci. U.S.A.* **2006**, *103*, 14901-14906.

14. Jansson, P. J.; Yamagishi, T.; Arvind, A.; Seebacher, N.; Gutierrez, E.; Stacy, A.; Maleki, S.; Sharp, D.; Sahni, S.; Richardson, D. R. Di-2-pyridylketone 4,4-dimethyl-3-thiosemicarbazone (Dp44mT) overcomes multidrug resistance by a novel mechanism involving the hijacking of lysosomal P-glycoprotein (Pgp). *J. Biol. Chem.* **2015**, *290*, 9588-9603.

15. Richardson, D. R.; Kalinowski, D. S.; Richardson, V.; Sharpe, P. C.; Lovejoy, D. B.; Islam, M.; Bernhardt, P. V. 2-Acetylpyridine thiosemicarbazones are potent iron chelators and antiproliferative agents: Redox activity, iron complexation and characterization of their antitumor activity. *J. Med. Chem.* **2009**, *52*, 1459-1470.

16. Jansson, P. J.; Kalinowski, D. S.; Lane, D. J. R.; Kovacevic, Z.; Seebacher, N. A.; Sahni, S.; Merlot, A. M.; Richardson, D. R. The renaissance of polypharmacology in the development of anti-cancer therapeutics: Inhibition of the "triad of death" in cancer by di-2-pyridylketone thiosemicarbazones. *Pharmacol. Res.* **2015**, *100*, 255-260.

17. Bernhardt, P. V.; Sharpe, P. C.; Islam, M.; Lovejoy, D. B.; Kalinowski, D. S.; Richardson, D. R. Iron chelators of the dipyridylketone thiosemicarbazone class: precomplexation and transmetalation effects on anticancer activity. *J. Med. Chem.* **2009**, *52*, 407-415.

18. Jansson, P. J.; Sharpe, P. C.; Bernhardt, P. V.; Richardson, D. R. Novel thiosemicarbazones of the ApT and DpT series and their copper complexes: Identification of pronounced redox activity and characterization of their antitumor activity. *J. Med. Chem.* **2010**, *53*, 5759-5769.

19. Lovejoy, D. B.; Jansson, P. J.; Brunk, U. T.; Wong, J.; Ponka, P.; Richardson, D. R. Antitumor activity of metal-chelating compound Dp44mT is mediated by formation of a redox-active copper complex that accumulates in lysosomes. *Cancer Res.* **2011**, *71*, 5871-5880.

20. Jansson, P. J.; Hawkins, C. L.; Lovejoy, D. B.; Richardson, D. R. The iron complex of Dp44mT is redox-active and induces hydroxyl radical formation: an EPR study. *J. Inorg. Biochem.* **2010**, *104*, 1224-1228.

21. Kovacevic, Z.; Chikhani, S.; Lovejoy, D. B.; Richardson, D. R. Novel thiosemicarbazone iron chelators induce up-regulation and phosphorylation of the metastasis suppressor N-myc down-stream regulated gene 1: A new strategy for the treatment of pancreatic cancer. *Mol. Pharmacol.* **2011**, *80*, 598-609.

22. Fang, B. A.; Kovacevic, Z.; Park, K. C.; Kalinowski, D. S.; Jansson, P. J.; Lane, D. J. R.; Sahni, S.; Richardson, D. R. Molecular functions of the iron-regulated metastasis suppressor, NDRG1, and its potential as a molecular target for cancer therapy. *Biochim. Biophys. Acta* **2014**, *1845*, 1-19.

23. Le, N. T. V.; Richardson, D. R. Iron chelators with high antiproliferative activity up-regulate the expression of a growth inhibitory and metastasis suppressor gene: a link between iron metabolism and proliferation. *Blood* **2004**, *104*, 2967-2975.

24. Nurtjahja-Tjendraputra, E.; Fu, D.; Phang, J. M.; Richardson, D. R. Iron chelation regulates cyclin D1 expression via the proteasome: a link to iron deficiency–mediated growth suppression. *Blood* **2007**, *109*, 4045-4054.

25. Saletta, F.; Rahmanto, Y. S.; Siafakas, A. R.; Richardson, D. R. Cellular iron depletion and the mechanisms involved in the iron-dependent regulation of the growth arrest and DNA damage family of genes. *J. Biol. Chem.* **2011**, *286*, 35396-35406.

26. Fu, D.; Richardson, D. R. Iron chelation and regulation of the cell cycle: 2 mechanisms of posttranscriptional regulation of the universal cyclin-dependent kinase inhibitor p21CIP1/WAF1 by iron depletion. *Blood* **2007**, *110*, 752-761.

27. Boya, P.; Kroemer, G. Lysosomal membrane permeabilization in cell death. *Oncogene* **2008**, *27*, 6434-6451.

28. Benes, P.; Vetvicka, V.; Fusek, M. Cathepsin D—Many functions of one aspartic protease. *Crit. Rev. Oncol. Hematol.* **2008**, *68*, 12-28.

29. Johansson, A.-C.; Appelqvist, H.; Nilsson, C.; Kågedal, K.; Roberg, K.; Öllinger, K. Regulation of apoptosis-associated lysosomal membrane permeabilization. *Apoptosis* **2010**, *15*, 527-540.

30. Dekanski, D.; Todorović, T.; Mitić, D.; Filipović, N.; Polović, N.; Anđelković, K. High antioxidative potential and low toxic effects of selenosemicarbazone metal complexes. *J. Serb. Chem. Soc.* **2013**, *78*, 1503–1512.

31. Shen, H.; Zhu, H.; Song, M.; Tian, Y.; Huang, Y.; Zheng, H.; Cao, R.; Lin, J.; Bi, Z.; Zhong, W. A selenosemicarbazone complex with copper efficiently down-regulates the 90-kDa heat shock protein HSP90AA1 and its client proteins in cancer cells. *BMC Cancer* **2014**, *14*, 629.

32. Filipović, N.; Polović, N.; Rašković, B.; Misirlić-Denčić, S.; Dulović, M.; Savić, M.; Nikšić, M.; Mitić, D.; Anđelković, K.; Todorović, T. Biological activity of two isomeric N-heteroaromatic selenosemicarbazones and their metal complexes. *Monat. Chem.* **2014**, *145*, 1089-1099.

33. Gligorijević, N.; Todorović, T.; Radulović, S.; Sladić, D.; Filipović, N.; Gođevac, D.; Jeremić, D.; Anđelković, K. Synthesis and characterization of new Pt(II) and Pd(II) complexes with 2-quinolinecarboxaldehyde selenosemicarbazone: Cytotoxic activity evaluation of Cd(II), Zn(II), Ni(II), Pt(II) and Pd(II) complexes with heteroaromatic selenosemicarbazones. *Eur. J. Med. Chem.* **2009**, *44*, 1623-1629.

34. Kowol, C. R.; Eichinger, R.; Jakupec, M. A.; Galanski, M.; Arion, V. B.; Keppler, B. K. Effect of metal ion complexation and chalcogen donor identity on the antiproliferative activity of 2-acetylpyridine N,N-dimethyl(chalcogen)semicarbazones. *J. Inorg. Biochem.* **2007**, *101*, 1946-1957.

35. Pizzo, C.; Faral-Tello, P.; Salinas, G.; Flo, M.; Robello, C.; Wipf, P.; Graciela Mahler, S. Selenosemicarbazones as potent cruzipain inhibitors and their antiparasitic properties against Trypanosoma cruzi. *Med. Chem. Comm.* **2012**, *3*, 362-368.

36. Revenko, M. D.; Prisacari, V. I.; Dizdari, A. V.; Stratulat, E. F.; Corja, I. D.; Proca, L. M. Synthesis, antibacterial, and antifungal activities of 8-quinolinealdehyde chalcogensemicarbazones and their copper(II) complexes. *Pharm. Chem. J.* **2011**, *45*, 351-354.

37. Turk, S. R.; Shipman, C., Jr.; Drach, J. C. Structure-activity relationships among alpha-(N)-heterocyclic acyl thiosemicarbazones and related compounds as inhibitors of herpes simplex virus type 1-specified ribonucleoside diphosphate reductase. *J. Gen. Virol.* **1986**, *67*, 1625-1632.

38. Klayman, D. L.; Scovill, J. P.; Bartosevich, J. F.; Mason, C. J. 2-Acetylpyridine thiosemicarbazones. 3. Selenium analogs as potential antimalarial agents. *Eur. J. Med. Chem.* **1981**, *16*, 317-320.

39. Kalinowski, D. S.; Yu; Sharpe, P. C.; Islam, M.; Liao, Y.-T.; Lovejoy, D. B.; Kumar, N.; Bernhardt, P. V.; Richardson, D. R. Design, synthesis, and characterization of novel iron chelators: Structure−activity relationships of the 2-benzoylpyridine thiosemicarbazone series and their 3-nitrobenzoyl analogues as potent antitumor agents. *J. Med. Chem.* **2007**, *50*, 3716-3729.

40. Richardson, D. R.; Sharpe, P. C.; Lovejoy, D. B.; Senaratne, D.; Kalinowski, D. S.; Islam, M.; Bernhardt, P. V. Dipyridyl thiosemicarbazone chelators with potent and selective antitumor activity form iron complexes with redox activity. *J. Med. Chem.* **2006**, *49*, 6510-6521.

41. De Laeter, J. R.; Bohlke, J. K.; De Bievre, P.; Hidaka, H.; Peiser, H. S.; Rosman, K. J.; Taylor, P. D. P. Atomic weights of the elements: Review 2000 (IUPAC technical report). *Pur Appl. Chem.* **2003**, *75*, 683-800.

42. Richardson, D. R.; Tran, E. H.; Ponka, P. The potential of iron chelators of the pyridoxal isonicotinoyl hydrazone class as effective antiproliferative agents. *Blood* **1995**, *86*, 4295-4306.

43. Yuan, J.; Lovejoy, D. B.; Richardson, D. R. Novel di-2-pyridyl–derived iron chelators with marked and selective antitumor activity: in vitro and in vivo assessment. *Blood* **2004**, *104*, 1450-1458.

44. Ponka, P.; Beaumont, C.; Richardson, D. R. Function and regulation of transferrin and ferritin. *Semin. Hematol.* **1998**, *35*, 35-54.

45. Chen, Z.; Zhang, D.; Yue, F.; Zheng, M.; Kovacevic, Z.; Richardson, D. R. The iron chelators Dp44mT and DFO inhibit TGF-beta-induced epithelial-mesenchymal transition via up-regulation of N-Myc downstream-regulated gene 1 (NDRG1). *J. Biol. Chem.* **2012**, *287*, 17016-17028.

46. Richardson, D. R.; Baker, E. The uptake of iron and transferrin by the human malignant melanoma cell. *Biochim. Biophys. Acta* **1990**, *1053*, 1-12.

47. Richardson, D. R.; Ponka, P. The iron metabolism of the human neuroblastoma cell: lack of relationship between the efficacy of iron chelation and the inhibition of DNA synthesis. *J. Lab. Clin. Med.* **1994**, *124*, 660-671.

48. Lane, D. J.; Saletta, F.; Suryo Rahmanto, Y.; Kovacevic, Z.; Richardson, D. R. N-myc downstream regulated 1 (NDRG1) is regulated by eukaryotic initiation factor 3a (eIF3a) during cellular stress caused by iron depletion. *PLoS One* **2013**, *8*, e57273.

49. Yu, Y.; Rahmanto, Y. S.; Richardson, D. R. Bp44mT: an orally active iron chelator of the thiosemicarbazone class with potent anti-tumour efficacy. *Br. J. Pharmacol.* **2012**, *165*, 148-166.

50. Kovacevic, Z.; Sivagurunathan, S.; Mangs, H.; Chikhani, S.; Zhang, D.; Richardson, D. R. The metastasis suppressor, N-myc downstream regulated gene 1 (NDRG1), upregulates p21 via p53-independent mechanisms. *Carcinogenesis* **2011**, *32*, 732-740.

51. Liu, W.; Yue, F.; Zheng, M.; Merlot, A.; Bae, D. H.; Huang, M.; Lane, D.; Jansson, P.; Lui, G. Y.; Richardson, V.; Sahni, S.; Kalinowski, D.; Kovacevic, Z.; Richardson, D. R. The proto-oncogene c-Src and its downstream signaling pathways are inhibited by the metastasis suppressor, NDRG1. *Oncotarget* **2015**, *6*, 8851-8874.

52. Ghalayini, M. K.; Dong, Q.; Richardson, D. R.; Assinder, S. J. Proteolytic cleavage and truncation of NDRG1 in human prostate cancer cells, but not normal prostate epithelial cells. *Biosci. Rep.* **2013**, *33*.

53. Lui, G. Y.; Obeidy, P.; Ford, S. J.; Tselepis, C.; Sharp, D. M.; Jansson, P. J.; Kalinowski, D. S.; Kovacevic, Z.; Lovejoy, D. B.; Richardson, D. R. The iron chelator, deferasirox, as a novel strategy for cancer treatment: oral activity against human lung tumor xenografts and molecular mechanism of action. *Mol. Pharmacol.* **2013**, *83*, 179-190.

54. Bandyopadhyay, S.; Pai, S. K.; Gross, S. C.; Hirota, S.; Hosobe, S.; Miura, K.; Saito, K.; Commes, T.; Hayashi, S.; Watabe, M.; Watabe, K. The Drg-1 gene suppresses tumor metastasis in prostate cancer. *Cancer Res.* **2003**, *63*, 1731-1736.

55. Bandyopadhyay, S.; Pai, S. K.; Hirota, S.; Hosobe, S.; Takano, Y.; Saito, K.; Piquemal, D.; Commes, T.; Watabe, M.; Gross, S. C.; Wang, Y.; Ran, S.; Watabe, K. Role of the putative tumor metastasis suppressor gene Drg-1 in breast cancer progression. *Oncogene* **2004**, *23*, 5675-5681.

56. Guan, R. J.; Ford, H. L.; Fu, Y.; Li, Y.; Shaw, L. M.; Pardee, A. B. Drg-1 as a differentiation-related, putative metastatic suppressor gene in human colon cancer. *Cancer Res.* **2000**, *60*, 749-755.

57. Hanahan, D.; Weinberg, R. A. Hallmarks of cancer: the next generation. *Cell* **2011**, *144*, 646-674.

58. Ledru, S.; Boujtita, M. Electrocatalytic oxidation of ascorbate by heme-FeIII/heme-FeII redox couple of the HRP and its effect on the electrochemical behaviour of an L-lactate biosensor. *Bioelectrochemistry* **2004**, *64*, 71-78.

59. Myhre, O.; Andersen, J. M.; Aarnes, H.; Fonnum, F. Evaluation of the probes 2′,7′-dichlorofluorescin diacetate, luminol, and lucigenin as indicators of reactive species formation. *Biochem. Pharmacol.* **2003**, *65*, 1575-1582.

60. Ubezio, P.; Civoli, F. Flow cytometric detection of hydrogen peroxide production induced by doxorubicin in cancer cells. *Free Radic. Biol. Med.* **1994**, *16*, 509-516.

61. Knox, J.; Hotte, S.; Kollmannsberger, C.; Winquist, E.; Fisher, B.; Eisenhauer, E. Phase II study of Triapine in patients with metastatic renal cell carcinoma: a trial of the National Cancer Institute of Canada Clinical Trials Group (NCIC IND.161). *Invest. New Drugs* **2007**, *25*, 471-477.

62. Quach, P.; Gutierrez, E.; Basha, M. T.; Kalinowski, D. S.; Sharpe, P. C.; Lovejoy, D. B.; Bernhardt, P. V.; Jansson, P. J.; Richardson, D. R. Methemoglobin formation by Triapine, di-2-pyridylketone-4,4-dimethyl-3-thiosemicarbazone (Dp44mT), and other anticancer thiosemicarbazones: Identification of novel thiosemicarbazones and therapeutics that prevent this effect. *Mol. Pharmacol.* **2012**, *82*, 105-114.

63. Traynor, A. M.; Lee, J. W.; Bayer, G. K.; Tate, J. M.; Thomas, S. P.; Mazurczak, M.; Graham, D. L.; Kolesar, J. M.; Schiller, J. H. A phase II trial of triapine (NSC# 663249) and gemcitabine as second line treatment of advanced non-small cell lung cancer: Eastern Cooperative Oncology Group Study 1503. *Invest. New Drugs* **2010**, *28*, 91-97.

64. Murren, J.; Modiano, M.; Clairmont, C.; Lambert, P.; Savaraj, N.; Doyle, T.; Sznol, M. Phase I and pharmacokinetic study of triapine, a potent ribonucleotide reductase inhibitor, administered daily for five days in patients with advanced solid tumors. *Clin. Cancer Res.* **2003**, *9*, 4092-4100.

65. Nutting, C. M.; van Herpen, C. M.; Miah, A. B.; Bhide, S. A.; Machiels, J. P.; Buter, J.; Kelly, C.; de Raucourt, D.; Harrington, K. J. Phase II study of 3-AP Triapine in patients with recurrent or metastatic head and neck squamous cell carcinoma. *Ann. Oncol.* **2009**, *20*, 1275-1279.

66. Nicolini, C.; Belmont, A.; Parodi, S.; Lessin, S.; Abraham, S. Mass action and acridine orange staining: static and flow cytofluorometry. *J. Histochem. Cytochem.* **1979**, *27*, 102-113.

67. Rundquist, I.; Olsson, M.; Brunk, U. Cytofluorometric quantitation of acridine orange uptake by cultured cells. *Acta Pathol. Microbiol. Immunol. Scand. A* **1984**, *92*, 303-309.

68. Drew, R.; Miners, J. O. The effects of buthionine sulphoximine (BSO) on glutathione depletion and xenobiotic biotransformation. *Biochem. Pharmacol.* **1984**, *33*, 2989-2994.

69. Aruoma, O. I.; Halliwell, B.; Hoey, B. M.; Butler, J. The antioxidant action of N-acetylcysteine: its reaction with hydrogen peroxide, hydroxyl radical, superoxide, and hypochlorous acid. *Free Radic. Biol. Med.* **1989**, *6*, 593-597.

70. Lovejoy, D. B.; Sharp, D. M.; Seebacher, N.; Obeidy, P.; Prichard, T.; Stefani, C.; Basha, M. T.; Sharpe, P. C.; Jansson, P. J.; Kalinowski, D. S.; Bernhardt, P. V.; Richardson, D. R. Novel second-generation di-2-pyridylketone thiosemicarbazones show synergism with standard chemotherapeutics and demonstrate potent activity against lung cancer xenografts after oral and intravenous administration in vivo. *J. Med. Chem.* **2012**, *55*, 7230-7244.

71. Odenike, O. M.; Larson, R. A.; Gajria, D.; Dolan, M. E.; Delaney, S. M.; Karrison, T. G.; Ratain, M. J.; Stock, W. Phase I study of the ribonucleotide reductase inhibitor 3-aminopyridine-2-carboxaldehyde-thiosemicarbazone (3-AP) in combination with high dose cytarabine in patients with advanced myeloid leukemia. *Invest. New Drugs* **2008**, *26*, 233-239.

72. Yen, Y.; Margolin, K.; Doroshow, J.; Fishman, M.; Johnson, B.; Clairmont, C.; Sullivan, D.; Sznol, M. A phase I trial of 3-aminopyridine-2-carboxaldehyde thiosemicarbazone in combination with gemcitabine for patients with advanced cancer. *Cancer Chemother. Pharmacol.* **2004**, *54*, 331-342.

73. Liu, W.; Kovacevic, Z.; Jin, R.; Wang, P.; Yue, F.; Zheng, M.; Huang, M. L. H.; Jansson, P. J.; Richardson, V.; Kalinowski, D. S.; Lane, D. J. R.; Merlot, A. M.; Sahni, S.; Richardson, D. R. The molecular effect of metastasis suppressors on Src signaling and tumorigenesis: New therapeutic targets. *Oncotarget* **2015**, *In Press -27th Sept*.

74. Martinelli, R. A.; Hanson, G. R.; Thompson, J. S.; Holmquist, B.; Pilbrow, J. R.; Auld, D. S.; Vallee, B. L. Characterization of the inhibitor complexes of cobalt carboxypeptidase A by electron paramagnetic resonance spectroscopy. *Biochemistry* **1989**, *28*, 2251-2258.

75. Sheldrick, G. M. *SHELX97. Programs for Crystal Structure Analysis*, release 97-2; University of Gottingen, Gottingen, Germany, 1998.

76. Farrugia, L. J. ORTEP-3 for Windows - A Version of ORTEP-III with a Graphical User Interface (GUI). *J. Appl. Cryst.* **1997**, *30*, 565.

77. Richardson, D. R.; Milnes, K. The potential of iron chelators of the pyridoxal isonicotinoyl hydrazone class as effective antiproliferative agents II: The mechanism of action of ligands derived from salicylaldehyde benzoyl hydrazone and 2-hydroxy-1-naphthylaldehyde benzoyl hydrazone. *Blood* **1997**, *89*, 3025-3038.

78. Baker, E.; Richardson, D.; Gross, S.; Ponka, P. Evaluation of the iron chelation potential of hydrazones of pyridoxal, salicylaldehyde and 2-hydroxy-1-naphthylaldehyde using the hepatocyte in culture. *Hepatology* **1992**, *15*, 492-501.

79. Gao, J.; Richardson, D. R. The potential of iron chelators of the pyridoxal isonicotinoyl hydrazone class as effective antiproliferative agents, IV: the mechanisms involved in inhibiting cell-cycle progression. *Blood* **2001**, *98*, 842-850.

80. Dean, R. T.; Nicholson, P. The action of nine chelators on iron-dependent radical damage. *Free Radic. Res.* **1994**, *20*, 83-101.

81. Winterbourn, C. C.; Carrell, R. W. Oxidation of human haemoglobin by copper. Mechanism and suggested role of the thiol group of residue beta-93. *Biochem. J.* **1977**, *165*, 141-148.

Table 1. Selected bond lengths (Å) and angles (°) for selenosemicarbazone (Ap44mSe) and related thiosemicarbazone (Ap44mT) Cu^{II} complexes.

	[Cu(Ap44mSe)(OAc)]	[Cu(Ap44mT)(OAc)]	$[Cu_2(Ap44mSe)_3]^+$	$[Cu(Ap44mT)_2]$
Cu1-N1	2.036(3)	2.014(3)	2.045(5), 2.261(7)	2.216(4), 2.238(3)
Cu1-N2	1.958(3)	1.943(3)	1.970(5), 2.029(6)	1.998(3), 2.011(3)
Cu1-X1 (X=Se,S)	2.3715(6)	2.253(1)	2.416(1), 2.762(1)	2.378(1), 2.487(1)
Cu1-O1	1.929(3)	1.954(2)		
Cu2-N1C			2.047(6)	
Cu2-N2C			1.997(6)	
Cu2-Se1A			2.910(1)	
Cu2-Se1B			2.406(1)	
Cu2-Se1C			2.351(1)	
C8-X1 (X=Se,S)	1.892(4)	1.750(4)	1.884(7), 1.918(8), 1.934(9)	
N1-Cu1-O1	97.5(1)	96.2(1)		
N1-Cu1-X1 (X=Se, S)	162.31(9)	165.5(1)	165.0(2), 156.4 (2)	157.1(1), 150.98(9)
C8-X1-Cu1 (X=Se,S)	91.2(1)	94.7(1)	90.4(2), 86.1(3)	94.3(2), 92.0(2)
Cu1-Se1-Cu2			84.1(4), 87.6(4)	

Note: The bond lengths and angles for the Ap44mT Cu^{II} complex has been taken from [18] for comparison.

Table 2. IC_{50} (μM) values of DFO, Dp44mT and Ap44mT and the selenosemicarbazone, Ap44mSe, and their Fe and Cu complexes at inhibiting the growth of SK-N-MC neuroepithelioma cells, as determined by the MTT assay (72 h/37°C). Results are mean ± SD (minimum of 3 experiments). The *p* values were determined using Student's *t*-test and were used to compare the activity of the ligand to that of its complexes.

Ligand	Free ligands	[Fe(DFO)] or [$Fe(L)_2$]		[Cu(L)]		[$Cu(L)_2$]	
	IC_{50} (μM)	IC_{50} (μM)	*p* value	IC_{50} (μM)	*p* value	IC_{50} (μM)	*p* value
DFO	19.31 ± 2.77	>25	-	11.81± 0.55	$p<0.05$	11.44 ± 0.25	$p<0.01$
Dp44mT	0.007 ± 0.001	>0.8	-	0.017 ± 0.002	$p<0.001$	0.010 ± 0.001	$p<0.01$
Ap44mT	0.009 ± 0.001	>0.8	-	0.016 ± 0.001	$p<0.001$	0.010 ± 0.001	$p>0.05$
Ap44mSe	0.011 ± 0.001	>0.8	-	0.012 ± 0.003	$p>0.05$	0.011 ± 0.001	$p>0.05$

Table 3. IC_{50} (μM) values of Dp44mT, Ap44mT and Ap44mSe at inhibiting the growth of mortal MRC-5 fibroblasts in comparison to SK-N-MC neuroepithelioma cells, as determined by the MTT assay (72 h/37°C). Therapeutic index values represent the ratio of MRC-5 to SK-N-MC IC_{50} values. Notably, a high therapeutic index value indicates marked selectivity for neoplastic relative to normal mortal cells.

Ligand	IC_{50} (μM)		*p* value	*Therapeutic Index*
	SK-N-MC	MRC-5		
Dp44mT	0.007 ± 0.001	0.54 ± 0.21	$p<0.01$	77
Ap44mT	0.009 ± 0.001	0.45 ± 0.21	$p<0.01$	50
Ap44mSe	0.011 ± 0.001	2.10 ± 0.93	$p<0.05$	191

Figure Legends

Figure 1. Line drawings of the chemical structures of the Fe chelators: **(A)** desferrioxamine (DFO); **(B)** di-2-pyridylketone 4,4-dimethyl-3-thiosemicarbazone (Dp44mT); **(C)** 2-acetylpyridine 4,4-dimethyl-3-thiosemicarbazone (Ap44mT); and **(D)** 2-acetylpyridine 4,4-dimethyl-3-selenosemicarbazone (Ap44mSe).

Figure 2. ORTEP diagrams of the Cu complexes of Ap44mSe: **(A)** [Cu(Ap44mSe)(OAc)] and **(B)** $[Cu_2(Ap44mSe)_3]^+$ cation (30% probability ellipsoids shown).

Figure 3. Cyclic voltammograms of the Cu complexes of Ap44mSe: **(A)** [Cu(Ap44mSe)(OAc)] (1 mM) in MeCN:H_2O 7:3 (0.1 M Et_4NClO_4) at different sweep rates; **(B)** (bottom) [Cu(Ap44mSe)(OAc)] and (top) $[Cu_2(Ap44mSe)_3](ClO_4)$ (1 mM) in MeCN:H_2O 7:3 (0.1 M Et_4NClO_4) at a sweep rate of 400 mV s^{-1}; and **(C)** $[Cu_2(Ap44mSe)_3](ClO_4)$ (1 mM) in MeCN:H_2O 7:3 (0.1 M Et_4NClO_4) at sweep rates of 25, 50 and 100 mV s^{-1}; the first cycle is shown as a solid curve and the second cycle is shown as a dashed curve.

Figure 4. X-band (9.341 GHz) EPR spectra of: (top) [Cu(Ap44mSe)(OAc)] and (bottom) [Cu(Ap44mT)(OAc)] both as 1 mM solutions in DMF (T = 130 K).

Figure 5. Ap44mSe is an effective Fe chelator in terms of inducing cellular ^{59}Fe mobilization and inhibiting cellular ^{59}Fe uptake from transferrin, demonstrating activity that is far greater than DFO. (A) The effect of chelators (2.5 and 25 μM) on ^{59}Fe mobilization from prelabeled SK-N-MC neuroepithelioma cells. Cells were labeled with $^{59}Fe_2$-transferrin ($^{59}Fe_2$-Tf; [Tf] = 0.75 μM) for 3 h/37^{o}C, washed four times on ice, and then reincubated for 3 h/37^{o}C in the presence or absence of the chelators. The release of ^{59}Fe from the cells mediated by the chelators into the overlying medium was then assessed. **(B)** The effect of chelators (2.5 and 25 μM) on internalized

^{59}Fe uptake from $^{59}Fe_2$-transferrin ($^{59}Fe_2$-Tf) by SK-N-MC neuroepithelioma cells. Cells were incubated for 3 h/37^{o}C with $^{59}Fe_2$-Tf ([Tf] = 0.75 μM) in the presence or absence of the chelators. After this incubation, the cells were washed four times on ice, and then the internalization of ^{59}Fe into the cells was determined by incubation with the protease, Pronase (1 mg/mL) for 30 min/4^{o}C. Results are mean ± SD of 3 experiments with 3 determinations in each experiment.

Figure 6. Ap44mSe modulates the expression of the Fe-regulated genes, transferrin receptor - 1 (TfR1), ferritin or NDRG1 in: (A) SK-N-MC and (B) SK-Mel-28 cells. Cells were incubated with either control medium or medium containing DFO (100 μM), Dp44mT (10 μM), Ap44mT (10 μM) or Ap44mSe (10 μM) for 24 h/37°C, and western blotting was then performed. The blot is a typical experiment from 3 experiments, whereas the densitometry is mean ± SD (3 experiments). For statistical analysis, each treatment was compared with the untreated control; *$p < 0.05$, **$p < 0.01$, ***$p < 0.001$.

Figure 7. The Fe complex of Ap44mSe is not redox active as demonstrated by: (A) ascorbate oxidation, whereas its Cu complex is redox active as shown by the DCF assay (B). (A) The effect of the Fe^{III} complexes of chelators on ascorbate oxidation at Fe-binding ratios (IBEs) of 0.1, 1 and 3; **(B)** the DCF fluorescence assay was performed by incubating SK-N-MC cells with the chelator in the presence and absence of $FeCl_3$, $CuCl_2$, or the Cu chelator, tetrathiomolybdate (TM). Results are mean ± SD of 3 experiments with 3 determinations in each experiment. For statistical analysis, each treatment was compared with the untreated control; *$p < 0.05$, **$p < 0.01$, ***$p < 0.001$.

Figure 8. Ap44mSe and its Fe(III) and Cu(II) complexes are markedly less effective than Dp44mT at catalyzing MetHb generation in intact human RBCs. MetHb generation by DFO, Dp44mT, Ap44mT or Ap44mSe and their Fe(III) or Cu(II) complexes (25 μM) were examined *via*

UV-Vis spectrophotometry after a 3 h incubation at 37 °C. Results are mean ± SD (3 experiments). *p < 0.05, **p < 0.01, ***p < 0.001 *versus* the control; $^{\#\#}p$ < 0.01, $^{\#\#\#}p$ < 0.001 *versus* the corresponding Dp44mT ligand, Fe-, or Cu-Dp44mT complex.

Figure 9. The Ap44mSe-Cu complex, but not the ligand, induces acridine orange re-distribution from lysosomes (red) to the cytosol (green) and is potentiated by buthionine sulfoximine (BSO), but prevented by the anti-oxidant, *N*-acetyl-L-cysteine (NAC), or the non-toxic Cu chelator, tetrathiomolybdate (TM). (A) Acridine orange (AO) lysosomotropic assay after incubation with Dp44mT, Ap44mT, or Ap44mSe alone or with either: $FeCl_3$ or $CuCl_2$ in the presence or absence of BSO, NAC, or TM. Scale bar: 50 µm. **(B)** Quantification of red fluorescence with the image processing and analysis software, ImageJ v1.48. Results are typical of 3 experiments. *, *versus* control, p <0.05; **, *versus* control, p <0.01; ***, *versus* control, p<0.001.

Figure 10. The Cu complex of Ap44mSe mediates redistribution of soluble cathepsin D (green) from lysosomes that were labeled with Lamp2 (red) to the cytosol, decreasing co-localization (yellow) of the two labels. (A) Immunofluorescence study examining lysosomal cathepsin D (green) and lysosomes (labeled with Lamp 2; red) after incubation of SK-N-MC cells with Ap44mSe alone and/or $CuCl_2$ in the presence or absence of either: BSO, NAC, or TM for 30 min/37˚C. The nucleus is labeled with DAPI (blue). Representative images are from 3 experiments. Scale bar: 50 µm. **(B)** Quantification of green cathepsin D fluorescence with the image processing and analysis software, ImageJ v1.48. Results are typical of 3 experiments. ***, *versus* control, p<0.001.

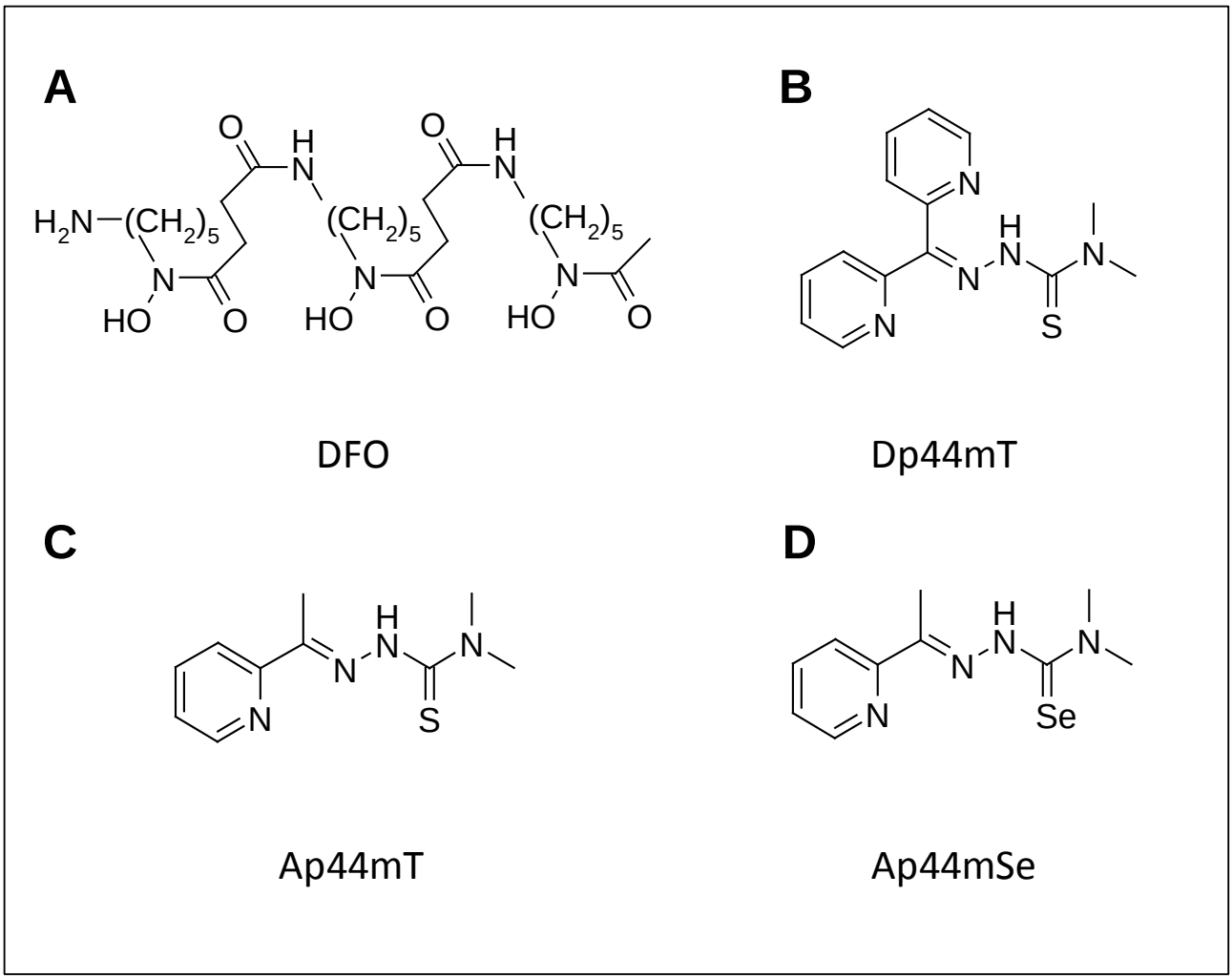

Figure 1

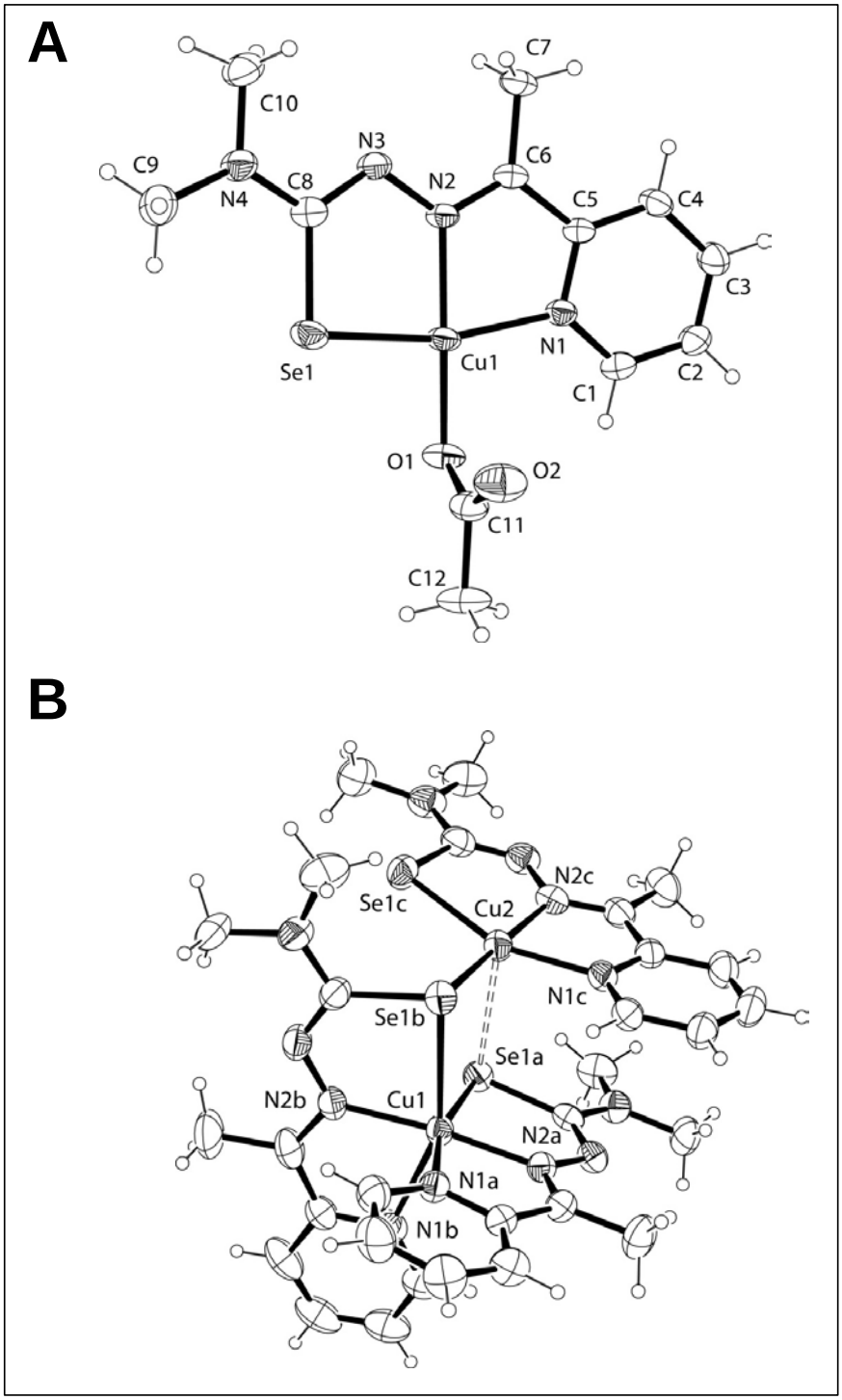
A
C7
C10
N3
C6
C9
C8
N2
C5
C4
N4
C3
N1
Se1
Cu1
C2
C1
O1
O2
C11
C12
B
N2c
Se1c
Cu2
N1c
Se1b
Se1a
N2b
Cu1
N2a
N1a
N1b

Figure 2

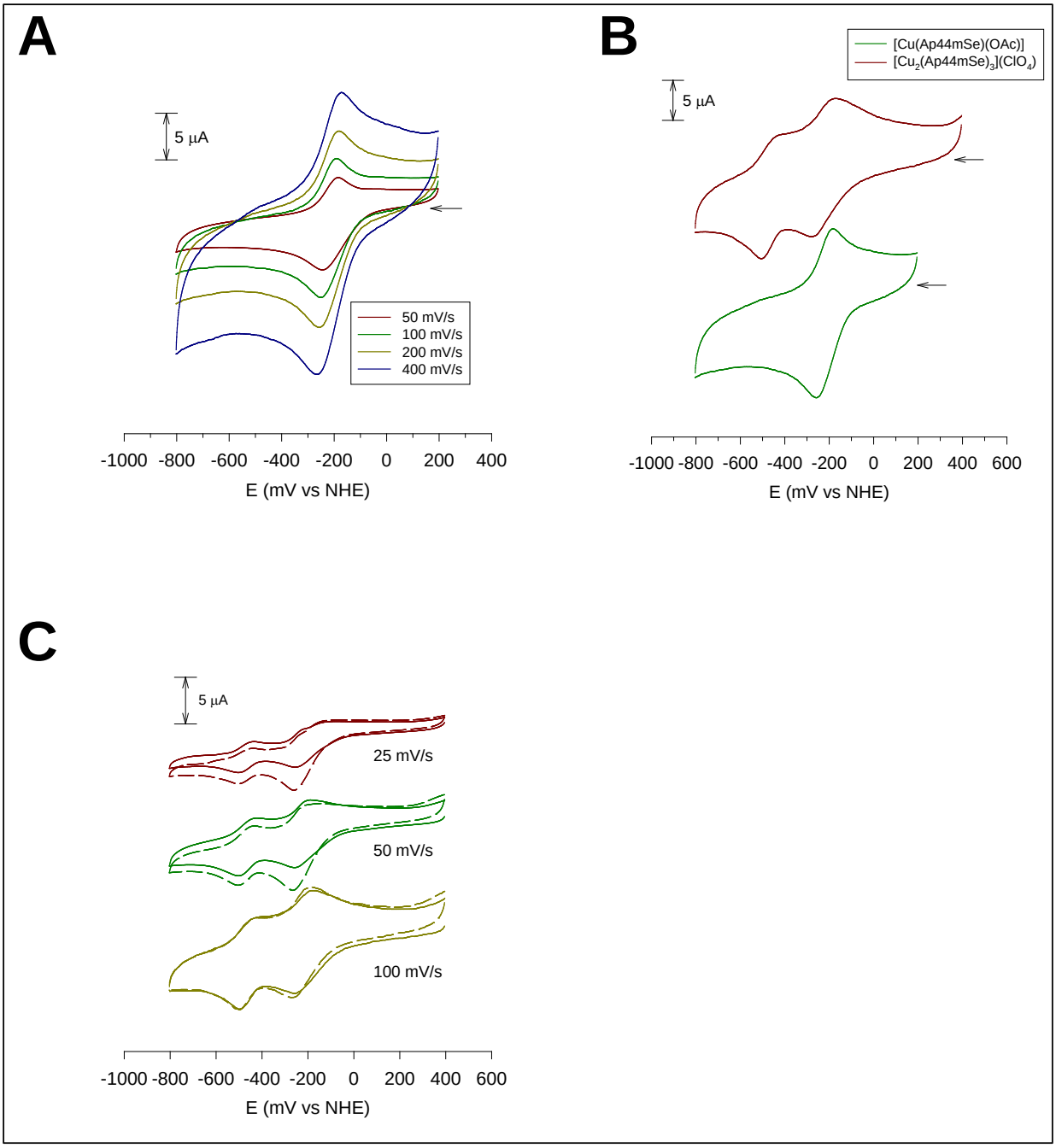
A
5 µA
50 mV/s
100 mV/s
200 mV/s
400 mV/s
-1000 -800 -600 -400 -200 0 200 400
E (mV vs NHE)
B
[Cu(Ap44mSe)(OAc)]
[Cu2(Ap44mSe)3](ClO4)
5 µA
-1000 -800 -600 -400 -200 0 200 400 600
E (mV vs NHE)
C
5 µA
25 mV/s
50 mV/s
100 mV/s
-1000 -800 -600 -400 -200 0 200 400 600
E (mV vs NHE)

Figure 3

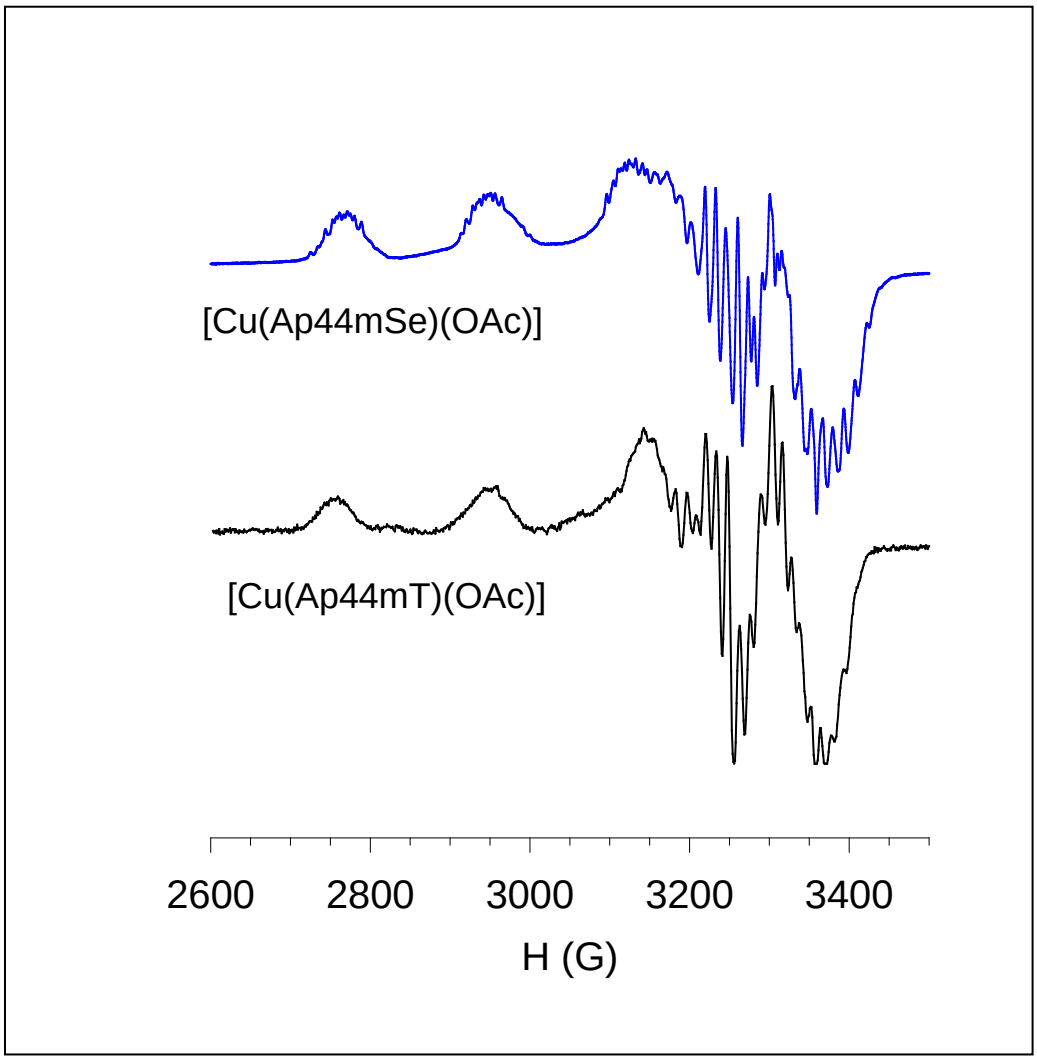

Figure 4

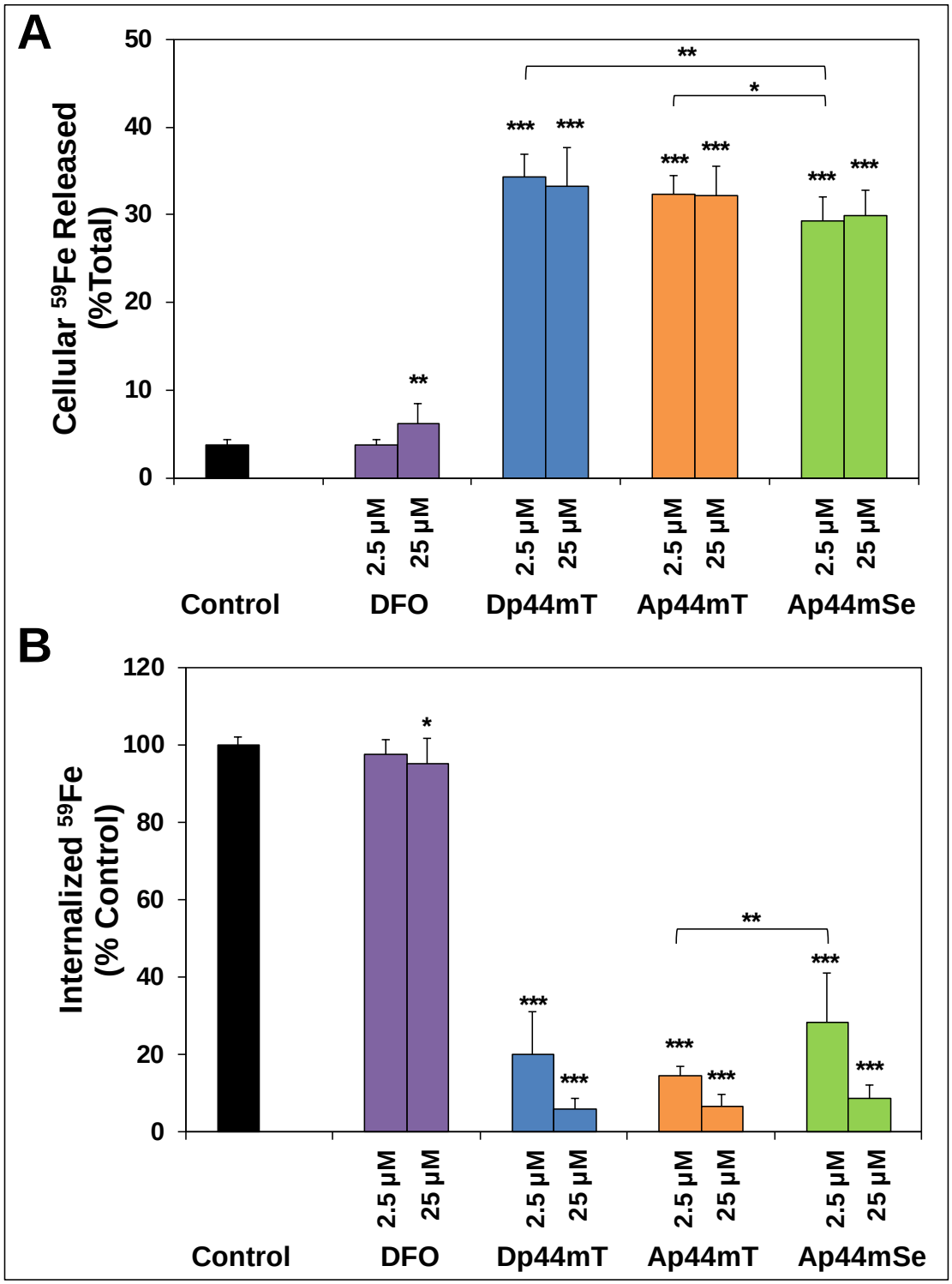
A
Cellular 59Fe Released (%Total)
50
40
30
20
10
0
**
*
***
***
***
***
***
***
**
2.5 µM
25 µM
Control
DFO
Dp44mT
Ap44mT
Ap44mSe
B
Internalized 59Fe (% Control)
120
100
80
60
40
20
0
*
**
***
***
***
***
***
***
2.5 µM
25 µM
Control
DFO
Dp44mT
Ap44mT
Ap44mSe

Figure 5

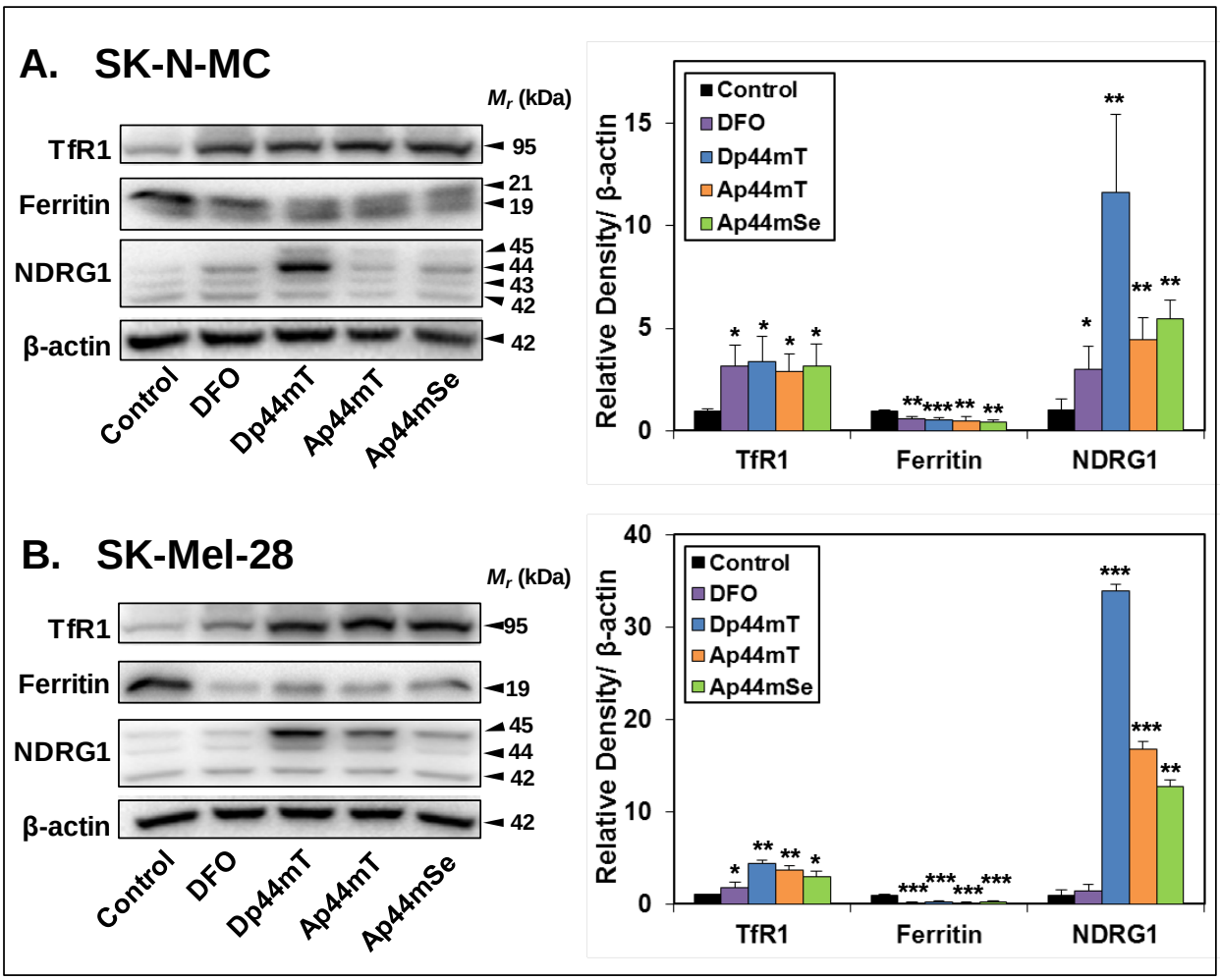
A. SK-N-MC
M_r (kDa)
TfR1
Ferritin
NDRG1
β-actin
95
21
19
45
44
43
42
42
Control
DFO
Dp44mT
Ap44mT
Ap44mSe
Relative Density/ β-actin
TfR1
Ferritin
NDRG1
B. SK-Mel-28
M_r (kDa)
TfR1
Ferritin
NDRG1
β-actin
95
19
45
44
42
42
Control
DFO
Dp44mT
Ap44mT
Ap44mSe
Relative Density/ β-actin
TfR1
Ferritin
NDRG1

Figure 6

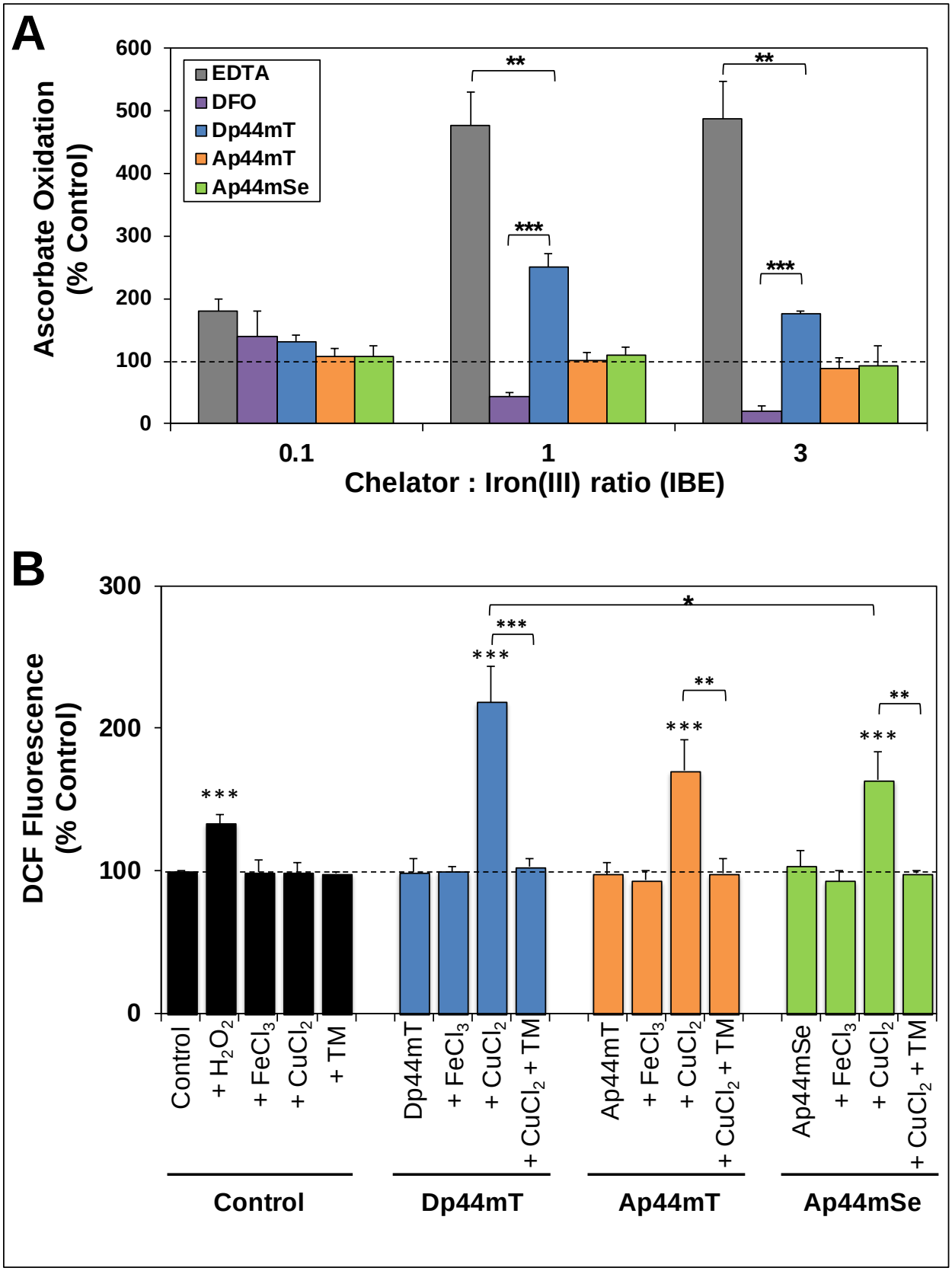
A
Ascorbate Oxidation (% Control)
600
500
400
300
200
100
0
EDTA
DFO
Dp44mT
Ap44mT
Ap44mSe
**
***
**
***
0.1
1
3
Chelator : Iron(III) ratio (IBE)
B
DCF Fluorescence (% Control)
300
200
100
0
***
***
***
*
**
***
**
***
Control
+ H2O2
+ FeCl3
+ CuCl2
+ TM
Dp44mT
+ FeCl3
+ CuCl2
+ CuCl2 + TM
Ap44mT
+ FeCl3
+ CuCl2
+ CuCl2 + TM
Ap44mSe
+ FeCl3
+ CuCl2
+ CuCl2 + TM
Control
Dp44mT
Ap44mT
Ap44mSe

Figure 7

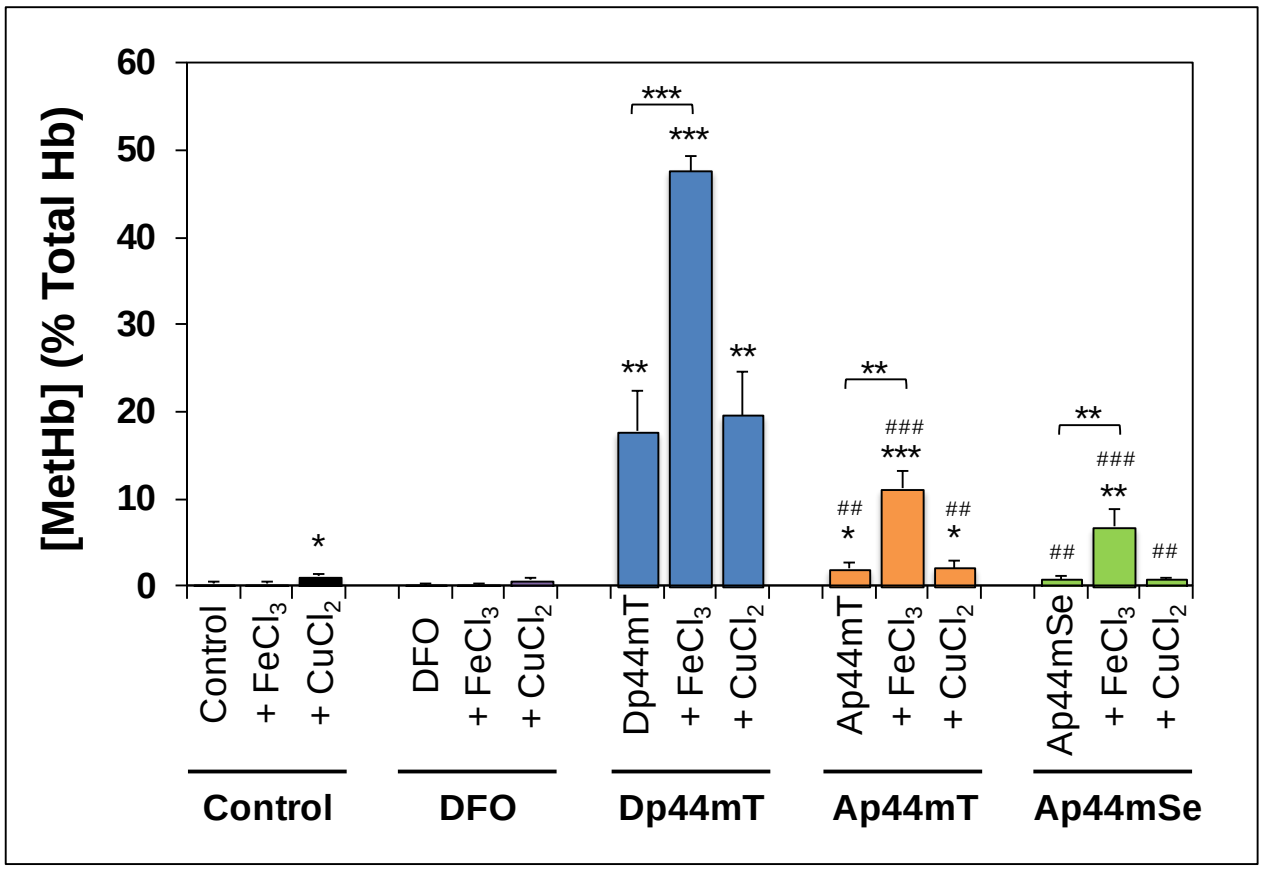
[MetHb] (% Total Hb)
60
50
40
30
20
10
0
Control
+ FeCl3
+ CuCl2
DFO
+ FeCl3
+ CuCl2
Dp44mT
+ FeCl3
+ CuCl2
Ap44mT
+ FeCl3
+ CuCl2
Ap44mSe
+ FeCl3
+ CuCl2
Control
DFO
Dp44mT
Ap44mT
Ap44mSe

Figure 8

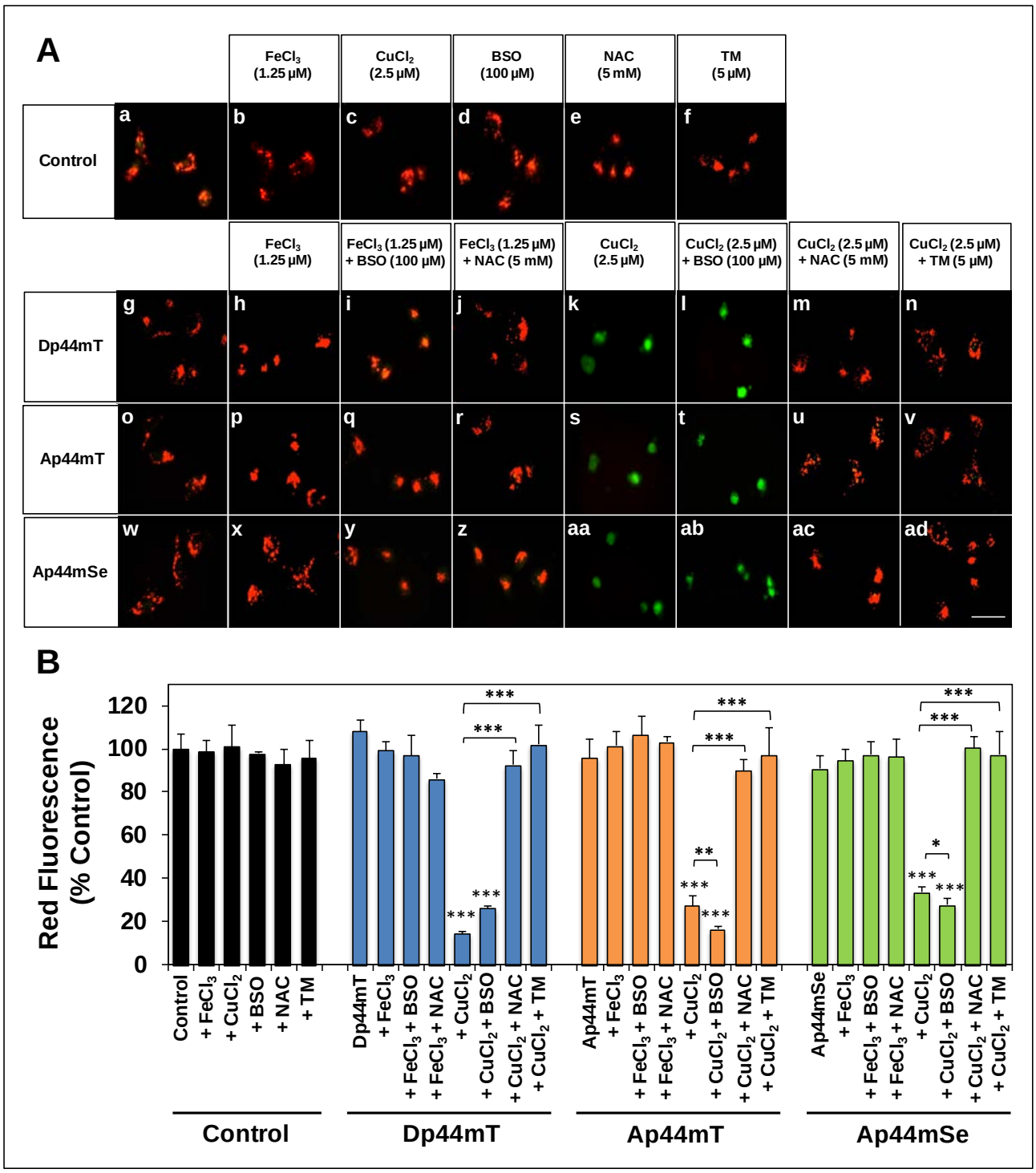
A
FeCl3 (1.25 µM)
CuCl2 (2.5 µM)
BSO (100 µM)
NAC (5 mM)
TM (5 µM)
Control
Dp44mT
Ap44mT
Ap44mSe
FeCl3 (1.25 µM) + BSO (100 µM)
FeCl3 (1.25 µM) + NAC (5 mM)
CuCl2 (2.5 µM) + BSO (100 µM)
CuCl2 (2.5 µM) + NAC (5 mM)
CuCl2 (2.5 µM) + TM (5 µM)
B
Red Fluorescence (% Control)
Control
Dp44mT
Ap44mT
Ap44mSe

Figure 9

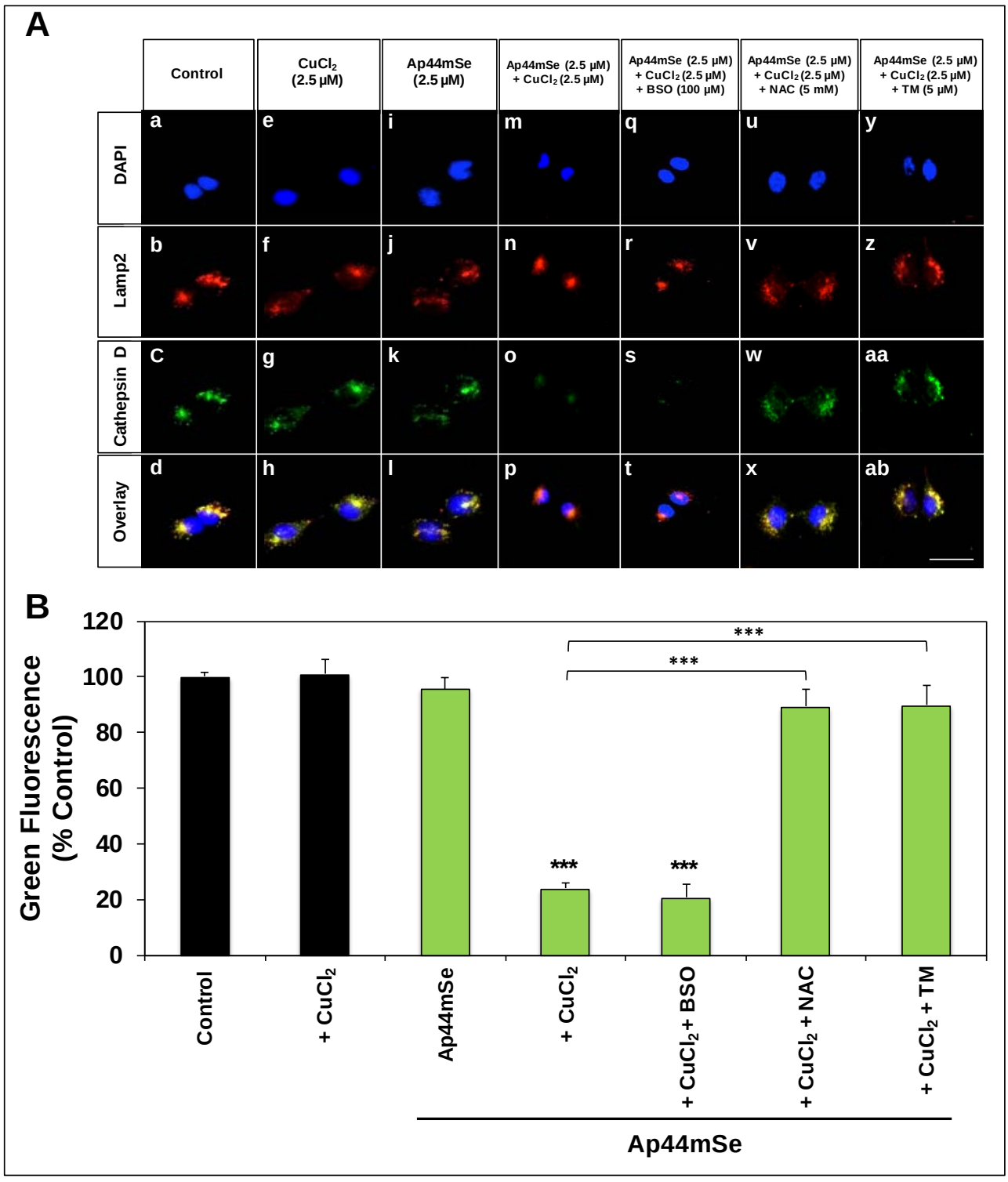
A
Control
CuCl2 (2.5 µM)
Ap44mSe (2.5 µM)
Ap44mSe (2.5 µM) + CuCl2 (2.5 µM)
Ap44mSe (2.5 µM) + CuCl2 (2.5 µM) + BSO (100 µM)
Ap44mSe (2.5 µM) + CuCl2 (2.5 µM) + NAC (5 mM)
Ap44mSe (2.5 µM) + CuCl2 (2.5 µM) + TM (5 µM)
DAPI
Lamp2
Cathepsin D
Overlay
a e i m q u y
b f j n r v z
C g k o s w aa
d h l p t x ab
B
Green Fluorescence (% Control)
120
100
80
60
40
20
0
***
***
***
***
Control
+ CuCl2
Ap44mSe
+ CuCl2
+ CuCl2 + BSO
+ CuCl2 + NAC
+ CuCl2 + TM
Ap44mSe

Figure 10

Table of Contents Graphic (TOC)